

MATHEMATISCHES FORSCHUNGSINSTITUT OBERWOLFACH

Report No. 37/2014

DOI: 10.4171/OWR/2014/37

## Mathematics and Algorithms in Tomography

Organised by  
Martin Burger, Münster  
Alfred K. Louis, Saarbrücken  
Eric Todd Quinto, Medford

10 August – 16 August 2014

**ABSTRACT.** This was the ninth Oberwolfach conference on the mathematics of tomography. Modalities represented at the workshop included X-ray tomography, radar, seismic imaging, ultrasound, electron microscopy, impedance imaging, photoacoustic tomography, elastography, emission tomography, X-ray CT, and vector tomography along with a wide range of mathematical analysis.

*Mathematics Subject Classification (2010):* 65R32, 44A12, 92C55.

### Introduction by the Organisers

Tomography includes a range of scientific modalities and underlying mathematics that provides information about internal structures of objects from indirect data: in medical imaging in a non-invasive way or in industrial environment in a non-destructive way. In these imaging modalities, the searched-for information is not directly accessible which means that one has to first setup a mathematical model relating the desired information with the available data and then to develop reconstruction formulas and algorithms reconstructing the information from the measured data.

Mathematics is fundamental to the field of tomography. Classical X-ray computed tomography became successful only when mathematics (including theory and algorithms) was developed for the problem. Since then, new imaging technologies have been invented and the dependence on mathematical results increased. Time dependent problems, vector-valued problems, novel integral transforms, and harmonic, numerical, and microlocal analysis, are among the ingredients in the basic mathematical research. The development of reconstruction methods relies on

these theoretical and numerical analytic results, allowing for algorithms superior to those found without this research.

The first Oberwolfach tomography workshop in 1980 helped define this young field. Many of the fundamental problems in the field were first articulated, in some form, at that meeting, and the subsequent Oberwolfach workshops have reflected the growing breadth of the area.

This year's workshop brought together 44 international experts, young scientists, and graduate students from Europe, North America, and Asia. The participants represented a broad range of areas from pure mathematics to numerical analysis to medicine and industry.

This ninth workshop mirrors the growth of the field. Modalities discussed include optical CT, magnetic resonance imaging, radar, seismic imaging, ultrasound, electron microscopy, impedance imaging, photoacoustic tomography, emission tomography, elastography, and vector tomography as well as X-ray CT. General algorithmic issues were discussed that are important in a range of tomography problems. Even in X-ray CT, one of the oldest modalities, new problems and mathematics were described as well as new views on algorithm development. New inversion methods were given for modalities including X-ray CT and thermoacoustic tomography. Several speakers provided novel reconstruction methods for dynamic CT, in which the body is moving, causing motion artifacts in standard reconstructions.

The analysis and mitigation of artifacts was another theme in the conference. Numerical analysis was used to analyze artifacts in cone beam CT. Speakers used microlocal methods to analyze the strength and location of artifacts in radar and photoacoustic tomography, providing a general methodology to characterize these artifacts, and precise estimates of the strength of the artifacts.

Fields including vector tomography, elastography, electron microscope tomography, PET, optical CT, and single photon emission tomography were explored algorithmically, by developing better physical models and in theoretical results. Time of flight PET was used to estimate attenuation and activity.

Summing up, tomography is a lively branch of science with an inexhaustible supply of mathematical problems. Every new imaging modality poses new mathematical questions, and new mathematics suggests new imaging modalities. This conference can be viewed as a snapshot of this lively field.

The organizers are indebted Prof. Dr. Huisken and the staff of the Mathematisches Forschungsinstitut Oberwolfach for creating an excellent environment to do serious mathematics. We thank the MFO for their efficient and very helpful organization that made the conference go smoothly and allowed us to focus on the mathematics. We thank the MFO also for supporting several young mathematicians through the OWLG program. Lastly, we thank the participants for making this a stimulating enjoyable conference.

*Acknowledgement:* The MFO and the workshop organizers would like to thank the National Science Foundation for supporting the participation of junior researchers in the workshop by the grant DMS-1049268, "US Junior Oberwolfach Fellows".

**Workshop: Mathematics and Algorithms in Tomography****Table of Contents**

Otmar Scherzer (joint with Peter Elbau, Leonidas Mindrinos) <i>Mathematical Modeling of Optical Coherence Tomography</i> .....	2053
Bernadette Hahn <i>Imaging moving objects</i> .....	2054
Alexander Katsevich (joint with Marco Bertola, Alexander Tovbis) <i>Finite Hilbert transform with incomplete data and the interior problem of tomography</i> .....	2057
Leonid Kunyansky <i>Inversion of the spherical means transform by reduction to the classical Radon transform</i> .....	2059
Per Christian Hansen <i>ART Exhibit</i> .....	2061
Clifford Nolan (joint with Raluca Felea) <i>Monostatic SAR with Fold-Cusp Singularities</i> .....	2063
Jürgen Friel (joint with Eric Todd Quinto) <i>Artifacts in limited view tomography</i> .....	2064
Gunther Uhlmann <i>Boundary rigidity and lens rigidity</i> .....	2066
Vladimir Sharafutdinov (joint with Jenn-Nan Wang) <i>Tomography of small residual stresses</i> .....	2072
Kees Joost Batenburg <i>Some steps in making tomography algorithms practical</i> .....	2073
Michel Defrise (joint with J. Nuyts, A. Rezaei, V. Panin, M. Caey, C. Michel, G. Bal, C. Watson, M. Conti) <i>Simultaneous estimation of attenuation and activity in time-of-flight positron emission tomography.</i> .....	2074
Steven Oeckl <i>New Inversion Formula for the X-ray transform and its Application to CT Reconstruction</i> .....	2076
S.K. Patch (joint with MCW team) <i>Thermoacoustics and the Spherical Radon Transform</i> .....	2078

Gaël Rigaud (joint with Aref Lakkhal) <i>Inversion of the attenuated Radon transform via circular harmonics expansions and contours reconstruction</i> . . . . .	2079
Holger Kohr (joint with T. Dahmen) <i>Mathematics of STEM tomography</i> . . . . .	2080
Ming Jiang (joint with Jason Cong, Yijin Guan, Peng Li, Guojie Luo, Peter Maaß, Thomas Page, Li Shen, Pei Wang, Peng Zhang, Wentai Zhang) <i>Methods for accelerating x-ray tomographic reconstruction</i> . . . . .	2083
John C. Schotland (joint with Guillaume Bal) <i>Acousto-Optic Inverse Source Problem</i> . . . . .	2085
Simon Arridge (joint with Matthias J. Ehrhardt) <i>Regularisation Methods for Joint Image Reconstruction</i> . . . . .	2087
Thomas Schuster (joint with Alexander Katsevich) <i>On an exact inversion formula for 3D cone beam vector tomography</i> . . .	2089
Carola-Bibiane Schönlieb (joint with Martin Benning, Lynn Gladden, Daniel Holland, Andy Sederman, Tuomo Valkonen) <i>Contrast-enhanced and sparse reconstruction for sub-sampled MR velocity imaging</i> . . . . .	2091
Samuli Siltanen (joint with Keijo Hämäläinen, Aki Kallonen, Ville Kolehmainen, Matti Lassas, Esa Niemi and Kati Niinimäki) <i>Multi-resolution method for choosing the total variation regularization parameter in X-ray tomography</i> . . . . .	2094
Andreas Rieder (joint with Robert Winkler) <i>Resolution-controlled conductivity discretization in electrical impedance tomography</i> . . . . .	2096
Victor Palamodov <i>Time reversal and Cormack's last paper</i> . . . . .	2098
Linh Nguyen <i>On artifacts in the limited data problem of spherical Radon Transform</i> .	2099
Frank Wübbeling (joint with Xiaoyi Jiang, Dirk Mannweiler, Julian Rasch, Klaus Schäfers, and Sönke Schmid) <i>PET imaging of freely moving mice via image registration</i> . . . . .	2100
Sebastian Suhr (joint with Martin Burger, Jan Modersitzki) <i>A Nonlinear Variational Approach to Motion-Corrected Reconstruction of Density Images</i> . . . . .	2102
Gaik Ambartsoumian (joint with Rim Gouia-Zarrad, Sunghwan Moon) <i>On the V-line Radon transform and its applications in imaging</i> . . . . .	2105

---

Ville Kolehmainen (joint with Jari P. Kaipio, Antti Nissinen)	
<i>Approximate marginalization of uninteresting unknowns in inverse problems</i> .....	2107
David Finch (joint with Patcharee Wongsason)	
<i>Cone beam transverse ray transform</i> .....	2107
Adel Faridani (joint with Ryan Hass)	
<i><math>\pi</math>-line reconstruction formulas in tomography: numerical analysis of view dependent derivatives</i> .....	2108
F. Alberto Grünbaum	
<i>Quantum walks with discrete time</i> .....	2110



## Abstracts

### Mathematical Modeling of Optical Coherence Tomography

OTMAR SCHERZER

(joint work with Peter Elbau, Leonidas Mindrinos)

We present a general mathematical model based on the electromagnetic theory for Optical Coherence Tomography (OCT).

OCT is a non-invasive imaging technique producing high-resolution images of biological tissues. It is based on Low (time) Coherence Interferometry measurements to image micro-structures with a resolution of a few micrometers. Standard OCT operates using broadband and continuous wave light in the visible and near-infrared spectrum. Images are obtained by measuring the time delay and the intensity of back-scattered or back-reflected light from the sample under investigation [2].

We describe mathematically the propagation of electromagnetic waves through an inhomogeneous sample with Maxwell's equations [1]. The sample is considered as a linear dielectric medium (inhomogeneous and anisotropic). Moreover, the medium is considered weakly scattering so that the first order Born approximation is applicable.

The optical properties of the medium are described by the (electric) susceptibility  $\chi : \mathbb{R} \times \mathbb{R}^3 \rightarrow \mathbb{R}^{3 \times 3}$ , assuming  $\chi(t < 0, x) = 0$ , and that is the quantity to be imaged. The time dependence of  $\chi$  hereby describes the fact that a change in the electric field cannot immediately cause a change in the electric displacement.

The measurements  $M$  are obtained by the combination of the back-scattered field from the sample and the back-reflected field from a reference mirror. In addition, the back-scattered light is detected far enough away from the sample so that the far field approximation can be assumed to be valid for the measurement data.

The mathematical formulation of the direct problem of OCT consists in simulating measurement data  $M$  of back-reflected waves for some  $\chi$ . These simulations can be written as an integral operator  $\mathcal{F} : \chi \mapsto M$ .

The inverse problem is to reconstruct the susceptibility of the medium given the measurements for different positions of the mirror. In mathematical terms we consider solving the operator equation

$$\mathcal{F}\chi = M.$$

With certain experimental design it is possible to express the measurement data as

$$(1) \quad p_j [\vartheta \times (\vartheta \times \tilde{\chi}(\omega, \frac{\omega}{c}(\vartheta + e_3))p)]_j, \quad j = 1, 2,$$

where  $p \in \mathbb{R}^2 \times \{0\}$  denotes the polarisation of the initial illumination,  $\omega \in \mathbb{R} \setminus \{0\}$  is the frequency and  $\vartheta \in S_+^2$  is the direction from the origin (where the sample

is located) to a detector point. Here  $\tilde{\chi}$  denotes the Fourier transform of  $\chi$  with respect to time and space.

In order to obtain  $\chi$  from (1) we consider different approaches depending on the different assumptions made about the optical properties of the sample. In the special case of an isotropic medium, meaning that the susceptibility matrix  $\chi$  is just a multiple of the unit matrix, it remains the problem of reconstructing the four dimensional susceptibility data from the three dimensional measurement data.

For non-dispersive media, where the temporal Fourier transform of  $\chi$  does not depend on frequency, several algorithms to recover the scalar susceptibility have been considered. In the case of a dispersive medium, we propose a recursive formula to get limited angle Radon data  $\bar{\chi}$  assuming a certain discretisation of  $\chi$  with respect to the detection points and its support. This procedure is applied to a full field OCT system and an extension to standard (time and frequency domain) OCT is briefly presented.

The anisotropic case is also considered and the proposed reconstruction method has to be combined with different initial polarisation vectors and rotations of the sample in order to provide sufficient information to reconstruct  $\bar{\chi}$ . Then, it is possible via an inversion of a limited angle Radon transform to recover the susceptibility  $\chi$ .

A detailed exposition of this topic can be found in [3].

#### REFERENCES

- [1] D. Colton and R. Kress. Inverse acoustic and electromagnetic scattering theory, volume 93 of Applied Mathematical Sciences. Springer-Verlag, Berlin, second edition, 1998.
- [2] W. Drexler and J. G. Fujimoto. Optical Coherence Tomography. Springer, Berlin, Heidelberg, 2008.
- [3] P. Elbau, L. Mindrinos and O. Scherzer. *Mathematical Modelling of Optical Coherence Tomography*, (to be published in Springer) arXiv:1403.0726 [math.NA].

### Imaging moving objects

BERNADETTE HAHN

The measuring process in tomographic imaging takes a considerable amount of time. In computerized tomography, for example, the X-ray source has to be rotated around the specimen. In positron emission tomography, the radioactive decay is observed over a certain time period. Analogously, this arises in MRI, EIT, etc. to name only a few. Most reconstruction methods for these imaging techniques make the assumption that the object is stationary during the data acquisition. However, in many applications, this supposition does not hold, e.g. in medical imaging due to respiratory and cardiac motion. A dynamic behavior of the specimen results in inconsistent data sets and the application of standard algorithms leads to motion artifacts in the images. Consequently, the reconstruction method has to take into account the deformations of the object.

Let the mathematical model for an imaging modality with a stationary object be given by an initial inverse problem

$$(1) \quad \mathcal{A}^{\text{stat}} h(t, y) = g(t, y)$$

with linear integral operator  $\mathcal{A}^{\text{stat}} : L_2(\Omega_X) \rightarrow L_2(\mathbb{R}_T \times \Omega_Y)$ .  $\Omega_X$  and  $\Omega_Y$  are compact subsets of  $\mathbb{R}^n$  and  $\mathbb{R}^m$ , respectively, and  $\mathbb{R}_T$  denotes the time interval covering the period required for the scanning. Thus, the model (1) already takes into account that the acquisition of the data  $g$  is time-dependent.

Consequently, an object  $f \in L_2(\mathbb{R}_T \times \Omega_X)$  which changes during the measuring procedure has to be recovered from the equation

$$(2) \quad \mathcal{A}f(t, y) = g(t, y),$$

with the dynamic operator

$$\mathcal{A}f(t, y) := \mathcal{A}^{\text{stat}} f_t(t, y), \quad t \in \mathbb{R}_T, y \in \Omega_Y.$$

According to the initial inverse problem (1), data for different values of  $t$  are required to reconstruct a stationary object. Thus, the measured data in the dynamic case cannot provide enough information to reconstruct the different states of the object properly. Therefore, we include an a priori information about the movement via diffeomorphic motion functions

$$\Gamma_t : \mathbb{R}^n \rightarrow \mathbb{R}^n,$$

where the value  $\Gamma_t x$  denotes which particle is at position  $x$  at time  $t$ .

Solving the inverse problem (2) requires a regularization scheme. Using the method of the approximate inverse [1], a mollified version of the solution,  $f^\gamma(t, x) = \langle f, e_{t,x}^\gamma \rangle$  is calculated from the measured data via

$$f^\gamma(t, x) = \langle g, \psi_{t,x}^\gamma \rangle,$$

where the *reconstruction kernel*  $\psi_{t,x}^\gamma$  is precomputed by solving  $\mathcal{A}^* \psi_{t,x}^\gamma = e_{t,x}^\gamma$ .

The a priori information about the motion model is incorporated by choosing the dynamic mollifier  $e_{t,x}^\gamma$  in accordance to the motion functions,

$$e_{t,x}^\gamma(v, z) = \left( \int_{\mathbb{R}_T} |\det D\Gamma_\tau^{-1}(\Gamma_v z)| d\tau \right)^{-1} \delta_{\Gamma_t x}^\gamma(\Gamma_v z)$$

with a given static mollifier  $\delta_x^\gamma \in L_2(\mathbb{R}^n)$  [2]. If  $e_{t,x}^\gamma$  is not in the range of the operator  $\mathcal{A}^*$ , we precompute the kernel  $\psi_{t,x}^\gamma$  by minimizing a Thikonov-Phillips functional, see [2]. By choosing the static mollifier  $\delta_x^\gamma$ , we can even compute features of the object, e.g. edges, directly from the measured data.

To illustrate the motion compensation property of the proposed algorithm, we apply the procedure in computerized tomography. In this case, the initial inverse problem (1) is given by the Radon transform  $\mathcal{R}$ . As numerical test object, we consider a locally changing chest phantom, whose initial state is shown in Figure 1. During the scanning, its heart is beating whereas the other organs are stationary.

To compensate for this local motion, we first have to determine which part of the object is affected by the deformation before applying the proposed reconstruction

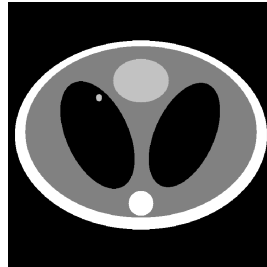


FIGURE 1. Original phantom at the initial time.

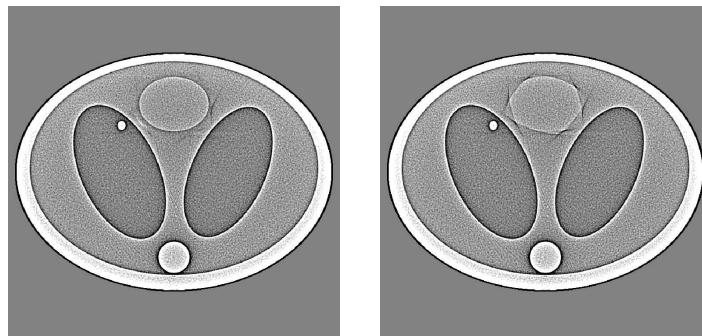


FIGURE 2. Dynamic (left) and static (right) reconstruction.

procedure. A suitable detection method is based on the symmetry property of the Radon transform  $\mathcal{R}$ ,

$$\mathcal{R}h(-\theta, -s) = \mathcal{R}h(\theta, s), \quad \theta \in S^1, s \in \mathbb{R}.$$

If the object changes locally, the symmetry condition does not hold on detector points  $s$  covering the dynamic region. Thus, we can determine which detector points record inconsistent data. Taking into account the respective angle of view, we obtain constraints for the dynamic area of the object [3].

This detection method is applied to the chest phantom and we use the derived information within the reconstruction process: For a reconstruction point  $x$  in the detected area, we incorporate the exact motion functions within a mollifier  $\delta_x^\gamma$  for the so-called Lambda tomography [4], as explained before. This yields local algorithms which are especially suitable in the case of local deformations. For reconstruction points outside the dynamic region, we use the respective stationary kernel [5].

Figure 2 shows the reconstruction result for the object's state at the initial time  $t = 0$ . The shape of the heart is reconstructed very well and there are hardly any distortion artefacts in the hearts vicinity. However, the standard algorithm in Lambda tomography leads to serious distortions of the heart, see Figure 3.

## REFERENCES

- [1] A. K. Louis, *Approximate inverse for linear and some nonlinear problems*, Inverse Problems **12** (1996), 175–90.
- [2] B. N. Hahn, *Efficient algorithms for linear dynamic inverse problems with known motion*, Inverse Problems **30** (2014), 035008(20pp).
- [3] B. N. Hahn, *Detecting locally changing objects from measured Radon data*, submitted.
- [4] F. Natterer, *The Mathematics of Computerized Tomography*, John Wiley & Sons, Chichester, 1986.
- [5] A. Rieder, R. Dietz and T. Schuster, *Approximate inverse meets local tomography*, Math. Meth. Appl. Sci. **23** (2000), 1373–87.

**Finite Hilbert transform with incomplete data and the interior problem of tomography**

ALEXANDER KATSEVICH

(joint work with Marco Bertola, Alexander Tovbis)

Inversion of the finite Hilbert transform (FHT) is an important problem, which arises in many areas of pure and applied mathematics. The work presented in this talk is motivated by the use of the FHT in tomography, which goes back to the Gelfand-Graev formula [4]. The Gelfand-Graev formula shows how to compute the Hilbert transform of an unknown function  $\mu$  knowing all line integrals of  $\mu$  (which are obtained from the tomographic data). Coupled with the FHT inversion formula, it leads to the development of new flexible reconstruction algorithms that require the minimum amount of CT data [10, 3, 14]. More recently it became clear that the Hilbert transform plays a key role in solving the so-called interior problem, which consists of reconstructing a region of interest (ROI) inside the support of  $\mu$  only from integrals of  $\mu$  along lines that intersect the ROI [13, 11, 12, 8, 2]. By using the Gelfand-Graev formula, the interior problem of tomography can be reduced to the problem of inverting the FHT from incomplete data. In [6, 7] the speaker found a differential operator  $L$  that commutes with the FHT on different intervals of a real line. A corollary to this result is a singular value decomposition (SVD) of the FHT [6, 7]. Based on the SVD, a robust algorithm for solving the interior problem of tomography was developed in [5]. In this talk we continue the analysis of the FHT and report on several recent results.

First we present the results obtained in [9]. Let  $f(x), x \in \mathbb{R}$ , be a compactly supported sufficiently smooth function, and  $\mathcal{H}$  denote the finite Hilbert transform. First we show that the commutation result can be derived by replacing the FHT of  $f$  with the Cauchy transform of  $f$  and appealing to the Riemann-Hilbert problem. Unique recovery of  $f$  is possible if  $\mathcal{H}f$  is known for all  $x \in \text{supp } f$ . Our second result is the characterization of the null-space of the FHT in the case of incomplete data, i.e. when  $\mathcal{H}f$  is known only on some interval inside  $\text{supp } f$ . The SVD of the FHT is obtained via solving certain singular Sturm-Liouville problems for  $L$ . Our next result is the uniform asymptotic expansion of the eigenfunctions of  $L$  as  $n \rightarrow \infty$ , where  $n$  is the index of the eigenfunction. Using this asymptotics we

derive the asymptotics of the singular values of the FHT in three different cases of incomplete data.

Next we present the results obtained in [1]. We study the asymptotics of singular values and singular functions of a Finite Hilbert transform (FHT), which is defined on several intervals. We suggest a novel approach based on the technique of the matrix Riemann-Hilbert problem and the steepest descent method of Deift-Zhou. We obtain a family of matrix RHPs depending on the spectral parameter  $\lambda$  and show that the singular values of the FHT coincide with the values of  $\lambda$  for which the RHP is not solvable. Expressing the leading order solution as  $\lambda \rightarrow 0$  of the RHP in terms of the Riemann Theta functions, we prove that the asymptotics of the singular values can be obtained by studying the intersections of the locus of zeroes of a certain Theta function with a straight line. This line can be calculated explicitly, and it depends on the geometry of the intervals that define the FHT. The leading order asymptotics of the singular functions and singular values are explicitly expressed in terms of the Riemann Theta functions and of the period matrix of the corresponding normalized differentials, respectively. We also obtain the error estimates for our asymptotic results.

#### REFERENCES

- [1] M. Bertola, A. Katsevich, and A. Tovbis, *Singular value decomposition of a finite Hilbert transform defined on several intervals and the interior problem of tomography: the Riemann-Hilbert problem approach*, Comm. Pure Appl. Math. **accepted** (2014), see also arXiv:1402.0216v1.
- [2] M. Courdurier, F. Noo, M. Defrise, and H. Kudo, *Solving the interior problem of computed tomography using a priori knowledge*, Inverse Problems **24** (2008), Article ID 065001, 27 pages.
- [3] M. Defrise, F. Noo, R. Clackdoyle, and H. Kudo, *Truncated Hilbert transform and image reconstruction from limited tomographic data*, Inverse Problems **22** (2006), 1037–1053.
- [4] I. M. Gelfand and M. I. Graev, *Crofton function and inversion formulas in real integral geometry*, Functional Analysis and its Applications **25** (1991), 1–5.
- [5] X. Jin, A. Katsevich, H. Yu, G. Wang, , L. Li, and Z. Chen, *Interior tomography with continuous singular value decomposition*, IEEE Trans. Med. Imag. **31** (2012), 2108–2119.
- [6] A. Katsevich, *Singular value decomposition for the truncated Hilbert transform*, Inverse Problems **26** (2010), article ID 115011 (12 pp).
- [7] ———, *A note on computing the derivative at a constant direction*, Physics in Medicine and Biology **56** (2011), N53–N61.
- [8] H. Kudo, M. Courdurier, F. Noo, and M. Defrise, *Tiny a priori knowledge solves the interior problem in computed tomography*, Phys. Med. Biol. **53** (2008), 2207–2231.
- [9] A. Katsevich and A. Tovbis, *Finite Hilbert transform with incomplete data: null-space and singular values*, Inverse Problems **28** (2012), no. 10, Article ID 105006, 28 pages.
- [10] F. Noo, R. Clackdoyle, and J. D. Pack, *A two-step Hilbert transform method for 2D image reconstruction*, Physics in Medicine and Biology **49** (2004), 3903–3923.
- [11] Y. B. Ye, H. Y. Yu, and G. Wang, *Exact interior reconstruction with cone-beam CT*, International Journal of Biomedical Imaging (2007), Article ID 10693.
- [12] ———, *Local reconstruction using the truncated Hilbert transform via singular value decomposition*, Journal of X-Ray Science and Technology **16** (2008), 243–251.
- [13] Y. Ye, H. Yu, Y. Wei, and G. Wang, *A general local reconstruction approach based on a truncated Hilbert transform*, International Journal of Biomedical Imaging (2007), Article ID 63634.

- [14] Y. Zou, X.C. Pan, and E.Y. Sidky, *Image reconstruction in regions-of-interest from truncated projections in a reduced fan-beam scan*, *Physics in Medicine and Biology* **50** (2005), 13–27.

### **Inversion of the spherical means transform by reduction to the classical Radon transform**

LEONID KUNYANSKY

Thermo- and photo- acoustic tomography (TAT and PAT) aim to recover initial pressure of acoustic wave from pressure time series measured on a certain surface partially or completely surrounding the region of interest. The wave is incited by illuminating the tissue with a very short laser pulse whose energy is partially absorbed by the tissue, which slightly increases the temperature and causes thermoacoustic expansion. The distribution of the initial pressure is closely related to the conductivity of the tissue, allowing one to reconstruct high resolution images of vasculature or cancerous tumors.

We are interested in finding exact closed-form reconstruction formulas for these imaging modalities. In addition to a clear theoretical insight, such formulas usually result in simple and efficient algorithms that allow one to reconstruct the initial pressure from the measured time series. In the context of thermo- and photo-acoustic tomography, the existence of explicit inversion formulas depends on the measurement surface. In particular, exact closed-form reconstruction formulas have been obtained for planes, infinite cylinders, spheres and ellipsoids; cubes, certain triangles and tetrahedra; paraboloids and two-sheet hyperboloids, and some other, more complicated surfaces.

In the present work we consider corner-like acquisition geometries, such as a boundary of an octant  $Q \equiv \{x \in \mathbb{R}^3 | x_1 > 0, x_2 > 0, x_3 > 0\}$  in 3D, or a boundary of a quadrant in 2D. Inversion formulas for such surfaces are of interest since the corresponding acquisition schemes are frequently used in practice. In particular, in order to speed up the measurements, researchers utilize one-dimensional assemblies of detectors combined with acoustical lenses. In common use are also optically scanned glass plates whose surfaces play roles of arrays of acoustic sensors. In order to see all the material interfaces, such detectors have to surround the region of interest (at least partially), resulting in the configurations considered here.

We assume that reflection of acoustic waves from the detectors is negligible. Such an assumption is realistic when detectors are small, or when a reflected wave propagates away from detectors and vanishes at infinity. In particular, if an optically scanned glass plate is used as a detector, the experiment should be repeated three times, with the glass plate placed in alternative positions. The use of several perpendicular glass plates simultaneously leads to occurrence of multiple reflections, and traditional TAT/PAT techniques are no longer applicable. Such a situation is not covered by the present work and is considered by the author elsewhere.

We present here the 3D version of the problem; the 2D version is simpler and can be solved quite similarly. Under assumption of constant speed of sound (that can be set to 1 without loss of generality), acoustic pressure  $u(t, x)$  satisfies the wave equation

$$\Delta u = u_{tt} \text{ in } \mathbb{R}^3, \quad u(0, x) = f(x), \quad \frac{\partial u}{\partial t}(0, x) = 0.$$

Initial pressure  $f(x)$  is supported within bounded region  $\Omega$  lying within the octant  $Q$ . Measurements  $g(t, z)$  coincide with pressure  $u(t, z)$  on boundary  $\partial Q$  of  $Q$  (the boundary is a subset of the three coordinate planes). Using the retarded Green's function  $G(t, z - x)$  of the wave equation in  $\mathbb{R}^3$  the measurements can be expressed in the following form

$$g(t, z) = \frac{\partial}{\partial t} \int_{\Omega} f(x) G(t, z - x) dx, \quad G(t, x) = \frac{\delta(t - |x|)}{4\pi|x|},$$

where  $\delta(t)$  is the Dirac's delta-function.

Consider the following combination of delta-functions supported on planes:

$$U(t, x) = \sum_{j=0}^7 (-1)^j \delta(t - x \cdot \omega^j),$$

where vectors  $\omega^j$  are multiple reflections the vector  $\omega^0 = (\omega_1, \omega_2, \omega_3) \in Q$ , and the signs in the above formula are chosen so that the distribution  $U(t, x)$  is odd with respect to each of the coordinates  $x_j$ ,  $j = 1, 2, 3$ . Let us denote by  $\partial Q_j$  the intersection of  $\partial Q$  with the coordinate plane  $x_j = 0$ ,  $j = 1, 2, 3$ . Then it can be shown that the inner product of  $f(x)$  and  $U_\delta(t, x, \omega)$  can be expressed through the measured data  $g(t, z)$  by the sum of the following three integrals:

$$(1) \quad \int_Q f(x) U_\delta(t, x, \omega) dx = 2(\omega_1 I_1 + \omega_2 I_2 + \omega_3 I_3),$$

$$I_1 = \int_{\partial Q_1} [g(t + y_2 \omega_3 + y_3 \omega_2, y) + g(t - y_2 \omega_3 - y_3 \omega_2, y) - g(t + y_2 \omega_3 - y_3 \omega_2, y) - g(t - y_2 \omega_3 + y_3 \omega_2, y)] dy,$$

where the expressions for integrals  $I_2$  and  $I_3$  are obtained from that for  $I_1$  by permuting roles of  $y_1$ ,  $y_2$ , and  $y_3$ , and the roles of  $\omega_1$ ,  $\omega_2$ , and  $\omega_3$ .

Further, one can show that inner product (1) coincides with the Radon transform of the odd part  $\mathcal{O}f$  of  $f(x)$ :

$$(\mathcal{R}\mathcal{O}f)(\omega, t) \equiv \int_{\mathbb{R}^3} \delta(t - x \cdot \omega) \mathcal{O}f(x) dx = \int_{\mathbb{R}^3} f(x) U_\delta(t, x, \omega) dx,$$

where  $\mathcal{O}f(x)$  is defined as

$$\begin{aligned} \mathcal{O}f(x) \equiv & f(x) - f(R_1 x) - f(R_2 x) - f(R_3 x) + f(R_2 R_1 x) + f(R_3 R_1 x) \\ & + f(R_3 R_2 x) - f(R_3 R_2 R_1 x), \end{aligned}$$

and where  $R_j$  are reflections of a vector with respect to coordinate planes  $x_j = 0$ ,  $j = 1, 2, 3$ . Since  $f(x)$  is supported within  $Q$ , it can be reconstructed from  $\mathcal{O}f(x)$  simply by restricting values of  $x$  to  $Q$ . It follows that  $f(x)$  can be explicitly reconstructed from the data  $g(t, z)$  by computing the values of the Radon transform  $(\mathcal{R}\mathcal{O}f)(\omega, t)$  using formula (1), and by applying to the result any of the known inversion formulas for the Radon transform in 3D.

### ART Exhibit

PER CHRISTIAN HANSEN

In Kaczmarz's formulation [6] of the algorithm from 1937, each iteration takes the form of a sweep over the rows  $a_i^T$  of the matrix  $A \in \mathbb{R}^{m \times n}$  – from top to bottom – where we orthogonally project the current iterate  $x$  on the hyperplane defined by row  $a_i^T$  and the corresponding element  $b_i$  of the right-hand side:

$$x \leftarrow \mathcal{P}_i x = x + \frac{b_i - a_i^T x}{\|a_i\|_2^2} a_i, \quad i = 1, 2, \dots, m.$$

Herman and his coworkers [3] rediscovered the algorithm 1970 (for the case where all elements of  $A$  are 0 or 1). They named it “ART,” introduced a nonnegativity projection and used a different normalization:

$$x \leftarrow \max \left\{ 0, x + \frac{b_i - a_i^T x}{\|a_i\|_1} a_i \right\}, \quad i = 1, 2, \dots, m.$$

This version does not have the simple interpretation as a sequence of orthogonal projections; in later works (e.g., [5]) the name ART is used synonymously with the Kaczmarz formulation. Current versions of ART also include a relaxation parameter  $\lambda_k$  and a projection  $\mathcal{P}_C$  on a convex set  $C$  (e.g., the positive orthant or the box  $[0, 1]^n$ ):

$$x \leftarrow \mathcal{P}_C \left( x + \lambda_k \frac{b_i - a_i^T x}{\|a_i\|_2^2} a_i \right), \quad i = 1, 2, \dots, m.$$

In spite of its success there are many open questions associated with the use of this method, and hence it is a rich source for research problems! Below two of some of these issues, with a strong bias towards my own research and my ongoing work with the MATLAB package AIR TOOLS [4]. Please note the effort by Joost Batenburt from CWI to develop a highly efficient toolbox ASTRA [9], based on a MATLAB wrapper around native C++ and CUDA code.

*Semi-Convergence Theory.* There is a rich convergence theory for ART and its many block extensions; but most of this theory exclusively deals with its asymptotic convergence. However, the power of ART really lies in its ability to converge fast to a good approximate/regularized solution during the initial iterations – while at later stages it slows down considerably and eventually converges to an undesirable solution dominated by noise from the data.

Specifically, ART is observed to exhibit *semi-convergence* [8], where the iteration number plays the role of the regularizing parameter. In the early stages the

iterates approach a regularized solution, while continuing the iteration leads to iterates deteriorated by noise. A few attempts have been made to give a rigorous foundation for this observed behavior, such as [1]; but more work is needed to demonstrate in which circumstances we are guaranteed to have semi-convergence, to give rates for the initial convergence, etc.

*Implementation of Block ART.* There are surprisingly many ways to define block extensions of ART; some of them are surveyed in [2] and [10]. These block methods lends themselves naturally to distributed computing systems and MPI-type implementations for large-scale problems [7]. The block methods are also well suited for multi-core computers [10] as well as systems based on GPUs. Some important questions here are:

- How do we best choose the number of blocks on a given computer?
- How can we best utilize the structural orthogonality between the matrix rows to choose the blocks adaptively?
- What is the best combination of block iteration (sequential/parallel) and treatment of the individual blocks (by a direct or iterative method)?

To best utilize the specialized architecture of the GPU, the matrix-free multiplications are implemented such that the backprojection corresponds to multiplication with the transposed of a matrix  $\tilde{A}$  that is slightly different from the matrix  $A$  associated with the forward computation [11]. The unmatched transpose may prevent asymptotic convergence; it is unclear how it affects the semi-convergence and the accuracy of the reconstruction.

#### REFERENCES

- [1] ELFVING, P. C. HANSEN, AND T. NIKAZAD, *Semi-convergence properties of Kaczmarz method*, Inverse Problems, 30 (2014), DOI: 10.1088/0266-5611/30/5/055007.
- [2] T. ELFVING, T. NIKAZAD, AND C. POPA, *A class of iterative methods: semi-convergence, stopping rules, inconsistency, and constraining*, in: Y. Censor, M. Jiang, and G. Wang (Eds.), *Biomedical Mathematics: Promising Directions in Imaging, Therapy Planning, and Inverse Problems*, Medical Physics Publishing, Madison, WI, 2010.
- [3] R. GORDON, R. BENDER, G. T. HERMAN, *Algebraic reconstruction techniques (ART) for three-dimensional electron microscopy and X-ray photography*, J. Theoretical Biology, 29 (1970), pp. 477–481.
- [4] P. C. HANSEN AND M. SAXILD-HANSEN, *AIR Tools – A MATLAB package of algebraic iterative reconstruction methods*, J. Comp. Appl. Math., 236 (2012), pp. 2167–2178, DOI: 10.1016/j.cam. 2011.09.039.
- [5] G. T. HERMAN, *Fundamentals of Computerized Tomography: Image Reconstruction from Projections*, 2. Ed., Springer, New York, USA, 2009.
- [6] S. KACZMARZ, *Angenäherte Auflösung von Systemen linearer Gleichungen*, Bull. Acad. Pol. Sci. Lett., A35 (1937), pp. 355–357.
- [7] N. T. KARONIS, K. L. DUFFIN, C. E. ORDOÑEZ, B. ERDELYI, T. D. URAM, E. C. OLSON, G. COUTRAKON, M. E. PAPKA, *Distributed and hardware accelerated computing for clinical medical imaging using proton computed tomography (pCT)*, J. Parallel Distrib. Comput., 73 (2013), pp. 1605–1612.
- [8] F. NATTERER, *The Mathematics of Computerized Tomography*, SIAM, Philadelphia, 2001.

- [9] W. J. PALENSTIJN, K. J. BATENBURG, AND J. SIJBERS, *Performance improvements for iterative electron tomography reconstruction using graphics processing units (GPUs)*, J. Structural Biology, 176 (2011), pp. 250–253.
- [10] H. H. B. SØRENSEN AND P. C. HANSEN, *Multi-core performance of block algebraic iterative reconstruction methods*, SIAM J. Sci. Comp., to appear.
- [11] G. L. ZENG AND G. T. GULLBERG, *Unmatched projector/backprojector pairs in an iterative reconstruction algorithm*, IEEE Trans. Medical Imag., 19 (2000), pp. 548–555.

### Monostatic SAR with Fold-Cusp Singularities

CLIFFORD NOLAN

(joint work with Raluca Felea)

In this talk we reported on preliminary work on imaging terrain using Synthetic Aperture Radar (SAR) where the flight track of the Radar follows a curve whose curvature is only allowed to vanish simply. For a microlocal review of SAR, see [1] and for related technical tools, see [3].

This work is a natural progression from [2] where the curvature of the flight track either (i) never vanishes or else (ii) is identically zero. In both cases (i) and (ii), the natural projections  $(\pi_L, \pi_R)$  from the wavefront relation  $\Lambda$  of the forward modelling (scattering) operator  $\mathcal{F}$  into the cotangent space of the data  $(T^*Y)$  and the cotangent space of the model  $(T^*X)$  respectively have singularities. In both case (i) and (ii) we have that  $\pi_L$  has a fold singularity. On the other hand, we have that the  $\pi_R$  projection has a fold singularity in case (i) and a blowdown singularity in case (ii). Both cases lead to artifacts in the backprojected image. This is reflected mathematically by showing that the Schwartz kernel of  $\mathcal{F}^*\mathcal{F}$  is a paired Lagrangian distribution associated to the diagonal  $\Delta$  and a non-diagonal canonical relation  $\Lambda$  (responsible for the artifacts).

In this current work [4], we investigate what happens in the intermediate case where the curvature is allowed to vanish but only simply. We establish that the Schwartz kernel of  $\mathcal{F}^*\mathcal{F}$  is no longer a paired Lagrangian distribution. We also show that artifacts are still present as this is intuitively clear if one considers say a sinusoid flight track with an inflexion point where the curvature vanishes simply. Now this flight track consists of two open curves where the curvature is never zero together with the inflexion point itself. Therefore we expect to obtain the artifacts predicted by [2].

We also develop a weak normal form for the phase function of the Fourier integral operator  $\mathcal{F}$  in the case of simply vanishing curvature and we use it to prove the results in the previous paragraph in a more general setting for any FIO with fold/cusp singularities.

#### REFERENCES

- [1] C.J. Nolan & M. Cheney. *Synthetic Aperture inversion. Inverse Problems. an International Journal on the Theory and Practice of Inverse Problems, Inverse Methods and Computerized Inversion of Data*, **18(1)**, (2002), 221–235.

- [2] C.J. Nolan & M. Cheney. *Microlocal analysis of synthetic aperture radar imaging*. The Journal of Fourier Analysis and Applications, **10(2)**, (2004), 133–148.
- [3] R. Felea, *Composition of Fourier integral operators with fold and blowdown singularities*. Communications in Partial Differential Equations, **30(10-12)**, (2005), 1717–1740.
- [4] R. Felea, C. Nolan, Monostatic SAR with fold/cusp singularities. Submitted

### Artifacts in limited view tomography

JÜRGEN FRIKEL

(joint work with Eric Todd Quinto)

**Introduction.** In many tomographic imaging scenarios the measured data is available only from a limited range of view. As a consequence, only specific features of the unknown object can be reconstructed reliably [11] and added artifacts can be generated [2, 6]. The added artifacts can degrade the image quality and complicate an accurate interpretation of images. It is therefore essential to develop a mathematical understanding of these phenomena and to derive artifact reduction strategies that can be easily incorporated into widely used reconstruction algorithms. Here, we consider filtered backprojection type reconstructions from limited view data and present a paradigm to characterize visible and added singularities (artifacts). Our methodology is based on the framework of microlocal analysis and the calculus of Fourier integral operators. Particularly, we present characterizations of visible and added singularities for limited angle x-ray and photoacoustic tomography reconstructions.

The presented results were obtained in our recent works [2, 3]. For x-ray lambda tomography similar results were obtained in [6]. Recently, L. Nguyen has analyzed the strength of the added artifacts generated in reconstructions from limited angle Radon transform and spherical Radon transform data [9, 10].

**Microlocal analysis of general limited data problems.** In what follows, we assume that the forward operator  $T : \mathcal{E}'(\Omega) \rightarrow \mathcal{E}'(\Xi)$  is a Fourier Integral operator (FIO), where  $\Omega$  denotes the object space and  $\Xi$  is the data space. The *limited data reconstruction problem* consists in recovering a function  $f$  (or an approximation) from the data  $g(y) = Tf(y)$  on a restricted subset  $A$  of the data space, i.e.,  $y \in A \subsetneq \Xi$ . Therefore, the limited view forward operator is given by  $T_A f = \chi_A T f$ , where  $\chi_A$  denotes the characteristic function of  $A$ . In cases we consider, the reconstruction operators  $B$  are of filtered backprojection (FBP) type:

$$Bg_A = T^* P g_A, \quad g_A = T_A f,$$

where  $P$  is a pseudodifferential operator and  $T^*$  is the dual (or backprojection) operator to  $T$ .

To understand visible and added singularities of  $Bg_A = T^* P T_A f$ , our goal is to calculate  $\text{WF}(T^* P T_A f)$ , where  $\text{WF}(u)$  denotes the wavefront set [4]. Before we can start the calculations, we first need to check that the product  $T_A f = \chi_A T f$  is well-defined in the sense of distributions. This can be done by making sure that the non-cancellation condition holds for  $\chi_A$  and  $T f$ , i.e.,  $(y, \xi) \in \text{WF}(T f) \Leftrightarrow$

$(y, -\xi) \notin \text{WF}(\chi_A)$ . In the next step we apply the Hörmander Sato lemma [12] which states that if  $T$  is a FIO and  $C$  its associated canonical relation, then  $\text{WF}(Tf) \subset C \circ \text{WF}(f) = \{(y, \eta \mathbf{d}y) : \exists(x, \xi \mathbf{d}x) \in \text{WF}(f) : (y, \eta \mathbf{d}y; x, \xi \mathbf{d}x) \in C\}$ . Furthermore, by noting that  $T^*$  is a FIO associated to the canonical relation  $C^t = \{(y, \eta \mathbf{d}y; x, \xi \mathbf{d}x) : (x, \xi \mathbf{d}x; y, \eta \mathbf{d}y) \in C\}$  [12], we conclude that

$$\text{WF}(T^*PT_Af) \subset C^t \circ \text{WF}(PT_Af) \subset C^t \circ \text{WF}(T_Af).$$

The latter inclusion follows from the pseudolocal property of pseudodifferential operators [12]. To compute visible and added singularities we eventually need to compute the set  $\text{WF}(T_Af)$  and the composition  $C^t \circ \text{WF}(T_Af)$ . For more details we refer to [3].

**Visible and added singularities in x-ray and photoacoustic tomography.**

We consider the classical Radon transform  $R : \mathcal{E}'(\Omega) \rightarrow \mathcal{E}'([0, 2\pi] \times \mathbb{R})$  as a forward operator for x-ray tomography, [8], and the limited angle data set  $A = [a, b] \times \mathbb{R}$ . The circular Radon transform  $M : \mathcal{E}'(\Omega) \rightarrow \mathcal{E}'([0, 2\pi] \times (0, \infty))$  is a standard forward operator for photoacoustic tomography, [1, 7], which we study with the limited angle data set  $A = [a, b] \times (0, \infty)$ . The next theorem shows explicitly that the Radon transforms detect singularities conormal to the set being integrated over (cf. [5]), and that added artifacts can appear only on lines (for  $R$ ) or circles (for  $M$ ), respectively, that are conormal to singularities of  $f$  with directions corresponding to the boundary of the angular range  $[a, b]$ .

**Theorem 1** ([2, 3]). *Let  $T \in \{R, M\}$ ,  $f \in \mathcal{E}'(\Omega)$ , and let  $P$  be a pseudodifferential operator on  $\mathcal{D}'(\Xi)$ . Then,*

$$\text{WF}(T^*PT_Af) \subset \text{WF}_{[a,b]}(f) \cup \mathcal{A}_{\{a,b\}}(f),$$

where  $\text{WF}_{[a,b]}(f) := \text{WF}(f) \cap \mathcal{V}_{[a,b]} \subset \text{WF}(f)$  is the set of visible singularities and  $\mathcal{A}_{\{a,b\}}(f)$  is the set of possible added singularities. Let  $\theta(\phi) = (\cos \phi, \sin \phi)$  and  $\theta^\perp(\phi) = (-\sin \phi, \cos \phi)$ , then we have for the classical Radon transform  $R$ :

$$\begin{aligned} \mathcal{V}_{[a,b]} &= \{(x, \xi \mathbf{d}x) \in T^*(\Omega) : \alpha \neq 0, \phi \in [a, b]\} \\ \mathcal{A}_{\{a,b\}}(f) &= \{(x + t\theta^\perp(\phi), \alpha\theta(\phi)\mathbf{d}x) : \phi \in \{a, b\}, \\ &\quad \alpha, t \neq 0, x \in L(\phi, s), (x, \alpha\theta(\phi)) \in \text{WF}(f)\} \end{aligned}$$

whereas for the circular Radon transform  $M$  we have:

$$\begin{aligned} \mathcal{V}_{[a,b]} &= \{(x, \xi \mathbf{d}x) \in T^*(\Omega) : \exists \phi \in [a, b], \exists \alpha \neq 0, \xi = \alpha(x - \theta(\phi))\} \\ \mathcal{A}_{\{a,b\}}(f) &= \{(x, d(x - \theta(\phi)\mathbf{d}x) : x \in \Omega, \phi \in \{a, b\}, \\ &\quad \exists x' \in C(\phi, \|x - \theta(\phi)\|), (x', d(x' - \theta(\phi))\mathbf{d}x) \in \text{WF}(f)\} \end{aligned}$$

The next theorem shows that no added singularities are introduced in the reconstruction if the limited view data is smoothly truncated at the boundary of the angular range.

**Theorem 2** ([2, 3]). *Let  $T \in \{R, M\}$  and let  $\kappa : [0, 2\pi] \rightarrow \mathbb{R}$  be a smooth function such that  $\text{supp}(\kappa) \subset [a, b]$ . Let  $\mathcal{K}$  be the operator defined by  $\mathcal{K}g(\phi, s) = \kappa(\phi)g(\phi, s)$ .*

Then, the operator  $T^*PKT_A$  is a standard pseudodifferential operator and for  $f \in \mathcal{E}'(D)$ ,

$$\text{WF}(T^*PK(T_A f)) \subset \text{WF}_{[a,b]}(f),$$

where  $\text{WF}_{[a,b]}(f)$  is the corresponding set of visible singularities given above.

#### REFERENCES

- [1] P. Elbau, O. Scherzer and R. Schulze, *Reconstruction formulas for photoacoustic sectional imaging*, Inverse Problems **28**(4): 045004, 2012.
- [2] J. Frikel and E. T. Quinto, *Characterization and reduction of artifacts in limited angle tomography*, Inverse Problems **29**(12): 125007, 2013.
- [3] J. Frikel and E. T. Quinto, *Artifacts in incomplete data tomography - with applications to photoacoustic tomography and sonar*, arXiv:1407.3453 [math.AP], 2014.
- [4] L. Hörmander, *The analysis of linear partial differential operators. I*, Springer-Verlag, Berlin, 2003.
- [5] V. Guillemin and S. Sternberg, *Geometric Asymptotics*, American Mathematical Society, Providence, RI, 1977.
- [6] A. Katsevich, *Local tomography for the limited-angle problem*, J. Math. Anal. Appl. **213**(1): 160-182, 1997.
- [7] P. Kuchment and L. Kunyansky, *Mathematics of photoacoustic and thermoacoustic tomography*, in Handbook of Mathematical Methods in Imaging, Otmar Scherzer, ed., Springer, 2010, pp. 817-866.
- [8] F. Natterer, *The mathematics of computerized tomography*, B. G. Teubner, Stuttgart, 1986.
- [9] L. Nguyen, *How strong are streak artifacts in limited angle computed tomography?*, arXiv:1407.3037 [math.CA], 2014.
- [10] L. Nguyen, *On Artifacts in Limited Data Spherical Radon Transform*, Preprint, 2014.
- [11] E. T. Quinto, *Singularities of the X-ray transform and limited data tomography in  $\mathbb{R}^2$  and  $\mathbb{R}^3$* , SIAM Journal on Mathematical Analysis **24**(5): 1215-1225, 1993.
- [12] F. Trèves, *Introduction to Pseudodifferential and Fourier Integral Operators*, Volume 2: Fourier Integral Operators, Plenum Press, New York and London, 1980.

### Boundary rigidity and lens rigidity

GUNTHER UHLMANN

#### ABSTRACT

We survey some recent results on the boundary rigidity problem with partial data based on [40]. The local result leads to a global result for the lens rigidity problem.

#### THE BOUNDARY RIGIDITY PROBLEM WITH PARTIAL DATA

Travel time tomography deals with the problem of determining the sound speed or index of refraction of a medium by measuring the travel times of waves going through the medium. This type of inverse problem, also called the inverse kinematic problem, arose in geophysics in an attempt to determine the substructure of the Earth by measuring the travel times of seismic waves at the surface. We consider an anisotropic index of refraction, that is the sound speed depends on the direction. The Earth is generally anisotropic. More recently it has been realized, by measuring these travel times, that the inner core of the Earth exhibits

anisotropic behavior with the fast direction parallel to the Earth's spin axis, see [4]. In the human body, muscle tissue is anisotropic. As a model of anisotropy, we consider a Riemannian metric  $g = (g_{ij})$ . The problem is to determine the metric from the lengths of geodesics joining points on the boundary.

This leads to the general question of whether given a compact Riemannian manifold with boundary  $(M, g)$  one can determine the Riemannian metric in the interior knowing the boundary distance function joining points on the boundary  $d_g(x, y)$ , with  $x, y \in \partial M$ . This is known as the *boundary rigidity problem*. Of course, isometries preserve distance, so that the boundary rigidity problem is whether two metrics that have the same boundary distance function are the same up to isometry. Examples can be given of manifolds that are not boundary rigid. Such examples show that the boundary rigidity problem should be considered under some restrictions on the geometry of the manifold. The most usual of such restrictions is simplicity of the metric. A Riemannian manifold  $(M, g)$  (or the metric  $g$ ) is called *simple* if the boundary  $\partial M$  is strictly convex and any two points  $x, y \in M$  are joined by a unique minimizing geodesic. Michel conjectured [17] that every simple compact Riemannian manifold with boundary is boundary rigid.

Simple surfaces with boundary are boundary rigid [24]. In higher dimensions, simple Riemannian manifolds with boundary are boundary rigid under some a-priori constant curvature on the manifold or special symmetries [1], [9]. Several local results near the Euclidean metric are known [32], [15], [2]. The most general result in this direction is the generic local (with respect to the metric) one proven in [34]. Surveys of some of the results can be found in [12], [35], [7].

The paper [40] considers the boundary rigidity problem in the class of metrics conformal to a given one and with partial data, that is, we know the boundary distance function for points on the boundary near a given point. Partial data problems arise naturally in applications since in many cases one doesn't have access to the whole boundary. In [40] it is proven the first result on the determination of the conformal factor locally near the boundary from partial data without assuming analyticity.

We now describe the known results with full data on the boundary. Let us fix the metric  $g_0$  and let  $c$  be a positive smooth function on the compact manifold with boundary  $M$ . The problem is whether we can determine  $c$  from  $d_{c^{-2}g_0}(x, y)$ ,  $x, y \in \partial M$ . Notice that in this case the problem is not invariant under changes of variables that are the identity at the boundary so that we expect to be able to recover  $c$  under appropriate a-priori conditions. This was proven by Mukhometov in two dimensions [19], and in [20] in higher dimensions for the case of simple metrics. Of particular importance in applications is the case of an isotropic sound speed that is when we are in a bounded domain of Euclidean space and  $g_0$  is the Euclidean metric. This is the isotropic case. This problem was considered by Herglotz [10] and Wieckert and Zoeppritz [43] for the case of a spherical symmetric sound speed. They found a formula to recover the sound speed from the boundary distance function assuming  $\frac{d}{dr}(\frac{r}{c(r)}) > 0$ . Notice that this condition is equivalent in the radial case to non-trapping and is more general than simplicity.

From now on we will call  $d$  the function  $d_{c^{-2}g_0}$ .

It is shown in [40] the following uniqueness result:

**Theorem 3.** *Let  $n = \dim M \geq 3$ , let  $c > 0$ ,  $\tilde{c} > 0$  be smooth and let  $\partial M$  be strictly convex with respect to both  $g = c^{-2}g_0$  and  $\tilde{g} = \tilde{c}^{-2}g_0$  near a fixed  $p \in \partial M$ . Let  $d(p_1, p_2) = \tilde{d}(p_1, p_2)$  for  $p_1, p_2$  on  $\partial M$  near  $p$ . Then  $c = \tilde{c}$  in  $M$  near  $p$ .*

This is the only known result for the boundary rigidity problem with partial data except in the case that the metrics are assumed to be real-analytic [15]. The latter follows from determination of the jet of the metric at a convex point from the distance function known near  $p$ .

#### LENS RIGIDITY

The boundary rigidity problem is closely connected to the lens rigidity one. To define the latter, we first introduce the manifolds  $\partial_{\pm}SM$ , defined as the sets of all vectors  $(x, v)$  with  $x \in \partial M$ ,  $v$  unit in the metric  $g$ , and pointing outside/inside  $M$ . We define the lens relation

$$(1) \quad L : \partial_-SM \longrightarrow \partial_+SM$$

in the following way: for each  $(x, v) \in \partial_-SM$ ,  $L(x, v) = (y, w)$ , where  $y$  is the exit point, and  $w$  the exit direction, if exist, of the maximal unit speed geodesic  $\gamma_{x,v}$  in the metric  $g$ , issued from  $(x, v)$ . Let

$$\ell : \partial_-SM \longrightarrow \mathbb{R} \cup \infty$$

be its length, possibly infinite. If  $\ell < \infty$ , we call  $M$  non-trapping.

The *lens rigidity* problem is whether the lens relation  $L$  (and possibly,  $\ell$ ) determine  $g$  (and the topology of  $M$ ) up to an isometry as above. The lens rigidity problem with partial data for a sound speed is whether we can determine the speed near some  $p$  from  $L$  known near  $S_p\partial M$ . For general metrics, we want to recover isometric copies of the metrics locally, as above.

We assume that  $\partial M$  is strictly convex at  $p \in \partial M$  w.r.t.  $g$ . Then the boundary rigidity and the lens rigidity problems with partial data are equivalent: knowing  $d$  near  $(p, p)$  is equivalent to knowing  $L$  in some neighborhood of  $S_p\partial M$ . The size of that neighborhood however depends on a priori bounds of the derivatives of the metrics with which we work. This equivalence was first noted by Michel [17], since the tangential gradients of  $d(x, y)$  on  $\partial M \times \partial M$  give us the tangential projections of  $-v$  and  $w$ , see also [31, sec. 2]. Note that local knowledge of  $\ell$  is not needed for either problems, and in fact,  $\ell$  can be recovered locally from either  $d$  or  $\ell$ .

Vargo [42] proved that real-analytic manifolds satisfying an additional mild condition are lens rigid. Croke has shown that if a manifold is lens rigid, a finite quotient of it is also lens rigid [7]. He has also shown that the torus is lens rigid [3]. G. Uhlmann and P. Stefanov have shown lens rigidity locally near a generic class of non-simple manifolds [37]. The only result we know for the lens rigidity problem with partial data is for real-analytic metric satisfying a mild condition [37]. While in [37], the lens relation is assumed to be known on a subset only, the

geodesics issued from that subset cover the whole manifold. In contrast, in [40], we have localized information.

The linearization of the boundary rigidity and lens rigidity problem is the tensor tomography problem, i.e., recovery of a tensor field up to “potential fields” from integrals along geodesics joining points on the boundary. It has been extensively studied in the literature for both simple and non-simple manifolds [8, 21, 22, 23, 18, 25, 30, 27, 33, 36, 39]. See the book [28] and [23] for a recent survey. The *local* tensor tomography problem has been considered in [13] for functions and real-analytic metrics and in [14] for tensors of order two and real-analytic metrics. Those results can also be thought of as support theorems of Helgason type. The only known results for the local problem for smooth metrics and integrals of functions is [41]. In [44] this type of result was proven for more general curves than geodesics and more general weights using similar methods.

Now we use a layer stripping type argument to obtain a global result which is different from Mukhometov’s for simple manifolds.

**Definition 1.** *Let  $(M, g)$  be a compact Riemannian manifold with boundary. We say that  $M$  satisfies the foliation condition by strictly convex hypersurfaces if  $M$  is equipped with a smooth function  $\rho : M \rightarrow [0, \infty)$  which level sets  $\Sigma_t = \rho^{-1}(t)$ ,  $t < T$  with some  $T > 0$  are strictly convex viewed from  $\rho^{-1}((0, t))$  for  $g$ ,  $d\rho$  is non-zero on these level sets, and  $\Sigma_0 = \partial M$  and  $M \setminus \cup_{t \in [0, T)} \Sigma_t$  has empty interior.*

The statement of the global result on lens rigidity proven in [40] is as follows:

**Theorem 4.** *Let  $n = \dim M \geq 3$ , let  $c > 0$ ,  $\tilde{c} > 0$  be smooth and equal on  $\partial M$ , let  $\partial M$  be strictly convex with respect to both  $g = c^{-2}g_0$  and  $\tilde{g} = \tilde{c}^{-2}g_0$ . Assume that  $M$  can be foliated by strictly convex hypersurfaces for  $g$ . Then if  $L = \tilde{L}$  on  $\partial_- SM$ , we have  $c = \tilde{c}$  in  $M$ .*

A more general foliation condition under which the theorem would still hold is formulated in [38]. In particular,  $\Sigma_0$  does not need to be  $\partial M$  and one can have several such foliations with the property that the closure of their union is  $M$ . If we can foliate only some connected neighborhood of  $\partial M$ , we would get  $c = \tilde{c}$  there. Note that it is enough to require that  $M \setminus \cup_{t \in [0, T)} \Sigma_t$  is simple to prove  $c = \tilde{c}$  in  $\cup_{t \in [0, T)} \Sigma_t$  first, and then use Mukhometov’s results to complete the proof. The class of manifolds we get in this way is larger than the simple ones.

Spherically symmetric  $c(x)$  under the condition considered by Herglotz and Wieckert and Zoeppritz satisfy the foliation condition of the theorem. Other examples of non-simple metrics that satisfy the condition are the tubular neighborhood of a closed geodesic in negative curvature. These have trapped geodesics. Also the rotationally symmetric spaces on the ball with convex spheres can be far from simple. It follows from the result of [26], that manifolds with no focal points satisfy the foliation condition. It would be interesting to know whether this is also the case for simple manifolds. As it was mentioned earlier manifolds satisfying the foliation condition are not necessarily simple.

The linearization of the non-linear problem with partial data considered in Theorem 3 was considered in [41], where uniqueness and stability were shown. This

corresponds to integrating functions along geodesics joining points in a neighborhood of  $p$ . The method of proof of Theorem relies on using an identity proven in [32] to reduce the problem to a "pseudo-linear" one: to show uniqueness when one integrates the function  $f =$  and its derivatives on the geodesics for the metric  $g$  joining points near  $p$ , with weight depending non-linearly on both  $g$  and  $\tilde{g}$ . Notice that this is not a proof by linearization, and unlike the problem with full data, an attempt to do such a proof is connected with essential difficulties. The proof of uniqueness for this linear transform follows the method of [41] introducing an artificial boundary and using Melrose' scattering calculus. The we use the method of [32] to reduce the problem to a "pseudo-linear problem" and apply similar techniques to [41].

#### STABILITY ESTIMATES

In Theorem 5 and Theorem 6 were proven in [40] giving a Hölder conditional stability estimates of local and then of global type respectively. In case of data on the whole boundary, such an estimate was proved in [34, section 7] for simple manifolds and metrics not necessarily conformal to each other. Below, the  $C^k$  norm is defined in a fixed coordinate system in the local result, and with respect to a fixed finite collection of local chart in the global case.

**Theorem 5.** *There exists  $k > 0$  and  $0 < \mu < 1$  with the following property. For any  $0 < c_0 \in C^k(M)$ ,  $p \in \partial M$ , and  $A > 0$ , there exists  $\varepsilon_0 > 0$  and  $C > 0$  with the property that for any two positive  $c, \tilde{c}$  with*

$$(2) \quad \|c - c_0\|_{C^2} + \|\tilde{c} - c_0\|_{C^2} \leq \varepsilon_0, \quad \text{and} \quad \|c\|_{C^k} + \|\tilde{c}\|_{C^k} \leq A, \quad j = 1, 2,$$

*and for any neighborhood  $\Gamma$  of  $p$  on  $\partial M$ , we have the stability estimate*

$$(3) \quad \|c - \tilde{c}\|_{C^2(U)} \leq \|d - \tilde{d}\|_{C(\Gamma \times \Gamma)}^\mu$$

*for some neighborhood  $U$  of  $p$  in  $M$ .*

The global estimate for the lens rigidity problem assuming the foliation condition is as follows:

**Theorem 6.** *Assume that  $M_0 \subset M$  can be foliated by strictly convex hypersurfaces. Let  $D \subset \partial_- SM$  be a neighborhood of the compact set of all  $\beta \in \partial_- SM \cap \partial_- SM_0$  with the property that the geodesic  $\gamma_\beta$  stays in  $M_0$  and hits  $\partial M$  again at a point on  $\partial M_0$ . Then with  $k, \mu, c_0, c, \tilde{c}, \varepsilon_0$  and  $A$  as in Theorem 5, we have the stability estimate*

$$(4) \quad \|c - \tilde{c}\|_{C^2(M_0)} \leq C \|L - \tilde{L}\|_{C(D)}^\mu$$

*for  $c_1, c_2$  satisfying (2).*

The quantity  $L - \tilde{L}$ , and its  $C(D)$  norm make sense in a finite system of charts covering  $\partial M$ .

#### ACKNOWLEDGEMENT

The Author was partly supported by the NSF and a Simons Fellowship.

## REFERENCES

- [1] G. Besson, G. Courtois, and S. Gallot. Entropies et rigidités des espaces localement symétriques de courbure strictement négative. *Geom. Funct. Anal.*, **5** (1995), 731–799.
- [2] D. Burago and S. Ivanov, Boundary rigidity and filling volume minimality of metrics close to a flat one. *Ann. Math.*, **171** (2010), 1183–1211.
- [3] C. Croke. Scattering rigidity with trapped geodesics. preprint, 2012.
- [4] K. C. Creager. Anisotropy of the inner core from differential travel times of the phases PKP and PKIPK, *Nature*, **356**(1992), 309–314.
- [5] C. B. Croke. Rigidity for surfaces of nonpositive curvature. *Comment. Math. Helv.*, **65**(1):150–169, 1990.
- [6] C. B. Croke. Rigidity and the distance between boundary points. *J. Differential Geom.*, **33**(2):445–464, 1991.
- [7] C. B. Croke. Rigidity theorems in Riemannian geometry. In *Geometric methods in inverse problems and PDE control*, volume 137 of *IMA Vol. Math. Appl.*, pages 47–72. Springer, New York, 2004.
- [8] N. S. Dairbekov. Integral geometry problem for nontrapping manifolds. *Inverse Problems*, **22**(2):431–445, 2006.
- [9] M. Gromov. Filling Riemannian manifolds. *J. Diff. Geometry* **18** (1983), 1–148.
- [10] G. Herglotz. Über die Elastizität der Erde bei Berücksichtigung ihrer variablen Dichte. *Zeitschr. für Math. Phys.*, **52**:275–299, 1905.
- [11] L. Hörmander. *The analysis of linear partial differential operators*, vol. 1-4. Springer-Verlag, 1983.
- [12] S. Ivanov. Volume comparison via boundary distances. *Proceedings of the International Congress of Mathematicians, vol. II*, 769–784, New Delhi, 2010.
- [13] V. Krishnan. A support theorem for the geodesic ray transform on functions. *J. Fourier Anal. Appl.* **15** (2009), 515–520.
- [14] V. Krishnan and P. Stefanov. A support theorem for the geodesic ray transform of symmetric tensor fields. *Inverse Problems and Imaging*, **3** (2009), 453–464.
- [15] M. Lassas, V. Sharafutdinov, and G. Uhlmann. Semiglobal boundary rigidity for Riemannian metrics. *Math. Ann.*, **325**(4):767–793, 2003.
- [16] R. B. Melrose. Spectral and scattering theory for the Laplacian on asymptotically Euclidian spaces. *Spectral and scattering theory (Sanda, 1992)*. Lecture Notes in Pure and Appl. Math., **161**, 85–130, Marcel Dekker, 1994.
- [17] R. Michel. Sur la rigidité imposée par la longueur des géodésiques. *Invent. Math.*, **65**(1):71–83, 1981/82.
- [18] R. G. Mukhometov. The reconstruction problem of a two-dimensional Riemannian metric, and integral geometry. *Dokl. Akad. Nauk SSSR*, **232**(1):32–35, 1977.
- [19] R. G. Muhometov. On a problem of reconstructing Riemannian metrics. *Sibirsk. Mat. Zh.*, **22**(3):119–135, 237, 1981.
- [20] R. G. Muhometov and V. G. Romanov. On the problem of finding an isotropic Riemannian metric in an  $n$ -dimensional space. *Dokl. Akad. Nauk SSSR*, **243**(1):41–44, 1978.
- [21] G.P. Paternain, M. Salo and G. Uhlmann. Tensor tomography on simple surfaces, *Invent. Math.*, **193**(2013), 229–247.
- [22] G.P. Paternain, M. Salo, G. Uhlmann. The attenuated ray transform for connections and Higgs fields, *Geom. Funct. Anal.* **22** (2012) 1460–1489.
- [23] G.P. Paternain, M. Salo and G. Uhlmann. Tensor tomography: progress and challenges, preprint, arXiv:1303.6114.
- [24] L. Pestov and G. Uhlmann. Two dimensional compact simple Riemannian manifolds are boundary distance rigid. *Ann. of Math. (2)*, **161**(2):1093–1110, 2005.
- [25] L. N. Pestov and V. A. Sharafutdinov. Integral geometry of tensor fields on a manifold of negative curvature. *Sibirsk. Mat. Zh.*, **29**(3):114–130, 221, 1988.

- [26] A. Ranjan and H. Shah. Convexity of spheres in a manifold without conjugate points. *Proc. Indian Acad. Sci. (Math. Sci.)*, **112** (2002), 595–599.
- [27] V. Sharafutdinov, M. Skokan, and G. Uhlmann. Regularity of ghosts in tensor tomography. *J. Geom. Anal.*, 15(3):499–542, 2005.
- [28] V. A. Sharafutdinov. *Integral geometry of tensor fields*. Inverse and Ill-posed Problems Series. VSP, Utrecht, 1994.
- [29] V. A. Sharafutdinov. A problem in integral geometry in a nonconvex domain. *Sibirsk. Mat. Zh.*, 43(6):1430–1442, 2002.
- [30] V.A. Sharafutdinov, Variations of Dirichlet-to-Neumann map and deformation boundary rigidity of simple 2-manifolds, *J. Geom. Anal.* **17** (2007), 147–187.
- [31] P. Stefanov. Microlocal approach to tensor tomography and boundary and lens rigidity. *Serdica Math. J.*, 34(1):67–112, 2008.
- [32] P. Stefanov and G. Uhlmann. Rigidity for metrics with the same lengths of geodesics. *Math. Res. Lett.*, 5(1-2):83–96, 1998.
- [33] P. Stefanov and G. Uhlmann. Stability estimates for the X-ray transform of tensor fields and boundary rigidity. *Duke Math. J.*, 123(3):445–467, 2004.
- [34] P. Stefanov and G. Uhlmann. Boundary rigidity and stability for generic simple metrics. *J. Amer. Math. Soc.*, 18(4):975–1003, 2005.
- [35] P. Stefanov and G. Uhlmann. Boundary and lens rigidity, tensor tomography and analytic microlocal analysis. In *Algebraic Analysis of Differential Equations*. Springer, 2008.
- [36] P. Stefanov and G. Uhlmann. Integral geometry of tensor fields on a class of non-simple Riemannian manifolds. *Amer. J. Math.*, 130(1):239–268, 2008.
- [37] P. Stefanov and G. Uhlmann. Local lens rigidity with incomplete data for a class of non-simple Riemannian manifolds. *J. Differential Geom.*, 82(2):383–409, 2009.
- [38] P. Stefanov and G. Uhlmann. Recovery of a source term or a speed with one measurement and applications, *Trans. Amer. Math. Soc.*, **365**, 5737–5758, 2013.
- [39] P. Stefanov and G. Uhlmann. The geodesic X-ray transform with fold caustics. *Anal. PDE*, **5**, 219–260, 2012.
- [40] P. Stefanov, G. Uhlmann and A. Vasy, Boundary rigidity with partial data, *preprint*, arXiv:1306.2995.
- [41] G. Uhlmann and A. Vasy. The inverse problem for the local geodesic ray transform. *preprint*, arXiv:1210.2084.
- [42] J. Vargo. A proof of lens rigidity in the category of analytic metrics, *Math. Research Letters*, **16** (2009), 1057–1069.
- [43] E. Wiechert and K. Zoeppritz. Über Erdbebenwellen. *Nachr. Koenigl. Gesellschaft Wiss. Göttingen*, 4:415–549, 1907.
- [44] H. Zhou. The inverse problem for the local ray transform. Preprint. arXiv:1304.7023, 2013.

### Tomography of small residual stresses

VLADIMIR SHARAFUTDINOV

(joint work with Jenn-Nan Wang)

We study the inverse problem of determining the residual stress in Man’s model [1] using tomographic data. Theoretically, the tomographic data are obtained at the zeroth approximation of geometrical optics for Man’s residual stress model. For compressional waves, the inverse problem is equivalent to the problem of inverting the longitudinal ray transform of a symmetric tensor field. For shear waves, the inverse problem, after the linearization, leads to another integral geometry operator which is called the mixed ray transform. Under some restrictions on coefficients, we are able to prove the uniqueness results in these two cases.

## REFERENCES

- [1] C.-S. Man. *Hartig's law and linear elasticity with initial stress*, *Inverse Problems* **14** (1998), 313–319.

**Some steps in making tomography algorithms practical**

KEES JOOST BATENBURG

In the past decades, X-ray tomography has developed into an advanced field of experimental research, utilizing not just the absorption contrast, but also phase, chemical and directional information to characterize the interior structure of the scanned object. Achieving the best possible results is becoming more and more an interdisciplinary effort, combining state-of-the-art experimental hardware, careful experiment design, mathematical modeling, customized algorithms and high performance computing.

One of the key challenges is to obtain accurate reconstructions from a limited set of measurements (a small number of projections, limited angular range, etc.). In this domain, recent mathematical advances in incorporating various types of prior knowledge in the reconstruction algorithm have the potential to provide vast improvements in image quality.

However, it is not at all straightforward to translate advanced numerical algorithms into a software implementation that can be applied effectively to large experimental datasets. In particular

- Practical data sets are often extremely large, requiring highly efficient parallel processing and efficient memory usage.
- A broad range of geometrical projection configurations is used in modern experiments, such that algorithms based on particular geometries (e.g. parallel beam, circular cone beam) can often not be used.
- A broad collection of structural errors and uncertainties introduced during image acquisition (alignment errors, flat field fluctuations, etc.) impose strong requirements on the robustness of the algorithm with respect to model errors.

At the Computational Imaging group of CWI (Amsterdam, The Netherlands) and the ASTRA group at the University of Antwerp (Belgium), we aim to develop methodologies that allow to bridge this gap between advanced mathematical algorithms and real-world experimental data. In particular, we have developed the ASTRA toolbox, an open-source software toolbox that offers flexible, high-performance GPU implementations of the tomographic forward and back projection operators [1, 2]. Through an interface with high-level scripting languages (Matlab and Python), algorithms can be expressed in an intuitive mathematical way, while being directly applicable to large experimental datasets.

## REFERENCES

- [1] W.J. Palenstijn, K.J. Batenburg, and J. Sijbers, *The ASTRA tomography toolbox*, 13th International Conference on Computational and Mathematical Methods in Science and Engineering, CMMSE, (2013). <http://sourceforge.net/projects/astra-toolbox/>.
- [2] W.J. Palenstijn, K.J. Batenburg, and J. Sijbers, *Performance improvements for iterative electron tomography reconstruction using graphics processing units (GPUs)*, Journal of Structural Biology, **176(2)** (2011), 250–253.

**Simultaneous estimation of attenuation and activity in time-of-flight positron emission tomography.**

MICHEL DEFRISE

(joint work with J. Nuyts, A. Rezaei, V. Panin, M. Caey, C. Michel, G. Bal, C. Watson, M. Conti)

Positron emission tomography (PET) aims at estimating the spatial distribution of a tracer labelled with a positron emitting isotope. This distribution, called the *activity image*  $\lambda$ , is reconstructed from the *emission data*  $m$ , which consist of pairs of 511 keV photons detected in coincidence by detectors surrounding the patient. An accurate reconstruction requires in addition information on the spatial distribution of the attenuation coefficient, (the *attenuation image*  $\mu$ ), which is needed to compensate for the absorption or scattering of the photons.

In practice the attenuation is measured independently using a CT scan (x-ray transmission tomography). However there are situations where the CT information is incomplete or inaccurate. The most common source of bias is the geometrical mismatch between the emission data and the attenuation image caused by patient motion or by different respiratory patterns in the CT and PET scans.

This talk describes recent results on the simultaneous estimation of the attenuation and activity images from time-of-flight (TOF) PET data, without using information from a CT or MR scan. This approach guarantees that the attenuation correction perfectly matches the PET data, both spatially and temporally. It is well known that the problem of simultaneously estimating the attenuation  $\mu(x)$ ,  $x \in \Omega \subset \mathbb{R}^3$  and activity  $\lambda(x)$  in PET has no unique solution [1]. We revisit this problem for time-of-flight (TOF) PET. Here, the data  $m$  depend on an additional TOF variable  $t$  equal to the time difference between the two coincident photons. In 2D,  $m(\phi, s, t) = a(\phi, s)p(\phi, s, t)$  for  $\phi \in [0, \pi)$ ,  $s, t \in \mathbb{R}$ , with

$$(1) \quad a(\phi, s) = \exp\{-(R\mu)(\phi, s)\} = \exp\left\{-\int dl \mu(s \cos \phi - l \sin \phi, s \sin \phi + l \cos \phi)\right\}$$

the *attenuation factor* along the line defined by the angle  $\phi$  and radial position  $s$ , and the non-attenuated data are

$$(2) \quad p(\phi, s, t) = \int dl \lambda(s \cos \phi - l \sin \phi, s \sin \phi + l \cos \phi) h(t - l)$$

with  $h(t)$  the probability distribution of the uncertainty on the measured time-of-flight. This function is usually, and in this work, modeled by a gaussian of

standard deviation  $\sigma$ . The non-attenuated data satisfy the range condition [2]

$$(3) \quad Dp = t \frac{\partial p}{\partial s} + \frac{\partial p}{\partial \phi} - s \frac{\partial p}{\partial t} + \sigma^2 \frac{\partial^2 p}{\partial s \partial t} = 0$$

By requiring that the corrected data  $p = m/a$  are in the range, and with weak smoothness assumptions, we show by solving  $D(m/a) = 0$  [3] that the gradient  $\nabla R\mu$  of the Radon transform of  $\mu$  is determined by the measured data  $m$  for all lines such that  $m(\phi, s) > 0$ . A corollary is that the solution of the TOF-PET simultaneous estimation is unique in the sense that

- the activity image  $\lambda$  is determined up to a global multiplicative constant,
- the attenuation factors  $a$  are determined for all lines which have activity, up to the reciprocal of the same multiplicative constant.

The proof is extended to 3D TOF-PET, where the data is function of 5 variables and satisfies two 2nd order partial differential equations, which generalize John's equation.

We also apply maximum likelihood (ML) estimation to a discrete version of this non-linear inverse problem with a Poisson likelihood model. Two approaches are discussed:

- The first one maximizes the likelihood with respect to  $\lambda$  and  $\mu$  [4]. This is done by alternatively updating  $\lambda$  and  $\mu$  using an algorithm originally introduced for non-TOF PET [5]. Similar techniques have been proposed for non-TOF PET [6, 7, 8], and recently [9] for TOF-PET.
- The second ML approach maximizes the likelihood with respect to  $\lambda$  and to the attenuation factors  $a$ . When the data are free of background (scatter and accidental coincidences), this second approach allows explicit optimization with respect to  $a$ , and we derive by optimization transfer a very simple monotonous algorithm to recover  $\lambda$ [10].

Examples with simulated and real PET data are presented.

#### REFERENCES

- [1] F. Natterer, *Determination of tissue attenuation in emission tomography of optically dense media*, Inverse Problems **9** (6) (1993) 731-736.
- [2] M. Defrise, V. Panin, C. Michel, M. Casey, *Continuous and Discrete Data Rebinning in Time-of-Flight PET*, IEEE Trans. Med. Imag. **27** (2008), 1310-1322.
- [3] M. Defrise, A. Rezaei, J. Nuyts, *Time-of-flight PET data determine the attenuation sinogram up to a constant*, Phys. Med. Biol. **57** (4) (2012), 885-899.
- [4] A. Rezaei, M. Defrise, G. Bal, C. Michel, M. Conti, C. Watson, J. Nuyts, *Simultaneous reconstruction of activity and attenuation in time-of-flight PET*, IEEE Trans. Med. Imag. **31** (12) (2012) 2224 - 2233.
- [5] J. Nuyts, P. Dupont, S. Stroobants, R. Benninck, L. Mortelmans, P. Suetens, *Simultaneous maximum a posteriori reconstruction of attenuation and activity distributions from emission sinograms*, IEEE Trans. Med. Imag. **18** (1999) 393-403.
- [6] Y. Censor, D. Gustafson, A. Lent, H. Tuy, *New approach to the emission computerized tomography problem: simultaneous calculation of attenuation and activity coefficients*, IEEE Trans. Nucl. Sc. **26** (2) (1979), 2775-2779.
- [7] H. Erdogan and J. Fessler, *Joint estimation of attenuation and emission images from PET scans*, Proc. IEEE Nucl. Sci. Symp. Med. Im. Conf. **3** (1999) 1672-1675.

- [8] N. Clinthorne, J. Fessler, G. Hutchins, W. Rogers, *Joint maximum likelihood estimation of emission and attenuation densities in PET*, Proc. IEEE Trans. Nucl. Sci. Symp. Med. Im. Conf. **3** (1991) 1927-1932.
- [9] S. Ahn, H. Qian, R. Manjeshwar, *Convergent iterative algorithms for joint reconstruction of activity and attenuation from time-of-flight PET data*, Records IEEE Nuclear Science Symposium and Medical Imaging Conference, Anaheim (2012), 3695-3700.
- [10] J. Nuyts, A. Rezaei, M. Defrise, *ML-reconstruction for TOF-PET with simultaneous estimation of the attenuation factors*, IEEE Trans. Med. Imag. **33** (7) (2014) 1563 - 1572.

## New Inversion Formula for the X-ray transform and its Application to CT Reconstruction

STEVEN OECKL

The (divergent) X-ray transform is the mathematical model for Computerized Tomography (CT). The two dimensional (2D) and the three dimensional (3D) X-ray transform is related to fan-beam and cone-beam CT, respectively. Analytical reconstruction algorithms are therefore based on the inversion of the X-ray transform especially for dimensions  $n \in \{2, 3\}$ . Instead of inverting the 2D X-ray transform usually the 2D Radon transform in combination with an appropriate transformation is used to derive reconstruction algorithms for fan-beam CT, see for example [1]. In case of cone-beam CT several inversion formulas for the 3D X-ray transform are well-known, see [2], [3], [4] [5], [6]. The mentioned formulas have all in common that one has to deal with the derivative of the Crofton symbol which is usually a discontinuous function and therefore causes numerical challenges. Here we present an inversion formula for the X-ray transform for arbitrary dimensions. Using this approach we avoid the derivative of the Crofton symbol.

Let  $n \in \mathbb{N}$  be a natural number with  $n \geq 2$  and let  $r \in \mathbb{R}^+$  be a positive real number. We define  $\mathbb{N}_0 := \mathbb{N} \cup \{0\}$ ,  $\mathbb{R}_*^n := \mathbb{R}^n \setminus \{0\}$ , and  $\Omega_r^n := \{x \in \mathbb{R}^n : \|x\| < r\}$  the open  $n$ -dimensional ball with radius  $r$ . Let  $S^{n-1} := \{x \in \mathbb{R}^n : \|x\| = 1\}$  be the  $n$ -dimensional unit sphere and  $H^\alpha(\Omega_r^n)$  the Sobolev space of order  $\alpha \in \mathbb{R}^+ \cup \{0\}$ . Let  $f$  be an appropriate function. We define the Fourier transform  $\hat{f} := (2\pi)^{-n/2} \int_{\Omega_r^n} f(x) e^{-i\langle x, \cdot \rangle} dx$  and for  $x \in \mathbb{R}^n$  the translation  $\mathcal{T}_x f := f(\cdot - x)$ . For  $f \in L^1(\mathbb{R}^n)$ ,  $a \in \mathbb{R}^n$ ,  $\theta \in S^{n-1}$  and  $k \in \mathbb{N}_0$  with  $k < n$  we define

$$\mathcal{D}^k f(a, \theta) := \mathcal{D}_a^k f := \int_0^\infty \rho^k f(a + \rho\theta) d\rho,$$

$$\mathcal{D}f(a, \theta) := \mathcal{D}_a f(\theta) := \mathcal{D}_a^0 f(\theta).$$

The operator  $\mathcal{D}$  is called *X-ray transform*. We call  $\mathcal{D}^k$  *generalized X-ray transform* and we define the abbreviation  $\mathcal{G}^k f(a, \theta) := \mathcal{G}_a^k f(\theta) := \mathcal{D}_a^k f(\theta) + \mathcal{D}_a^k f(-\theta)$ .

Let  $\Lambda \subset \mathbb{R}$  be a closed interval. The curve that corresponds to a path  $\phi : \Lambda \rightarrow \mathbb{R}^n$  is denoted by  $\Gamma_\phi := R(\phi) \subset \mathbb{R}^n$ . The set of all paths where the corresponding curve is lying outside of  $\Omega_r^n$  is defined by  $\Phi^{n,r}(\Lambda) := \{\phi : \Lambda \rightarrow \mathbb{R}^n \mid R(\phi) \subset \mathbb{R}^n \setminus \Omega_r^n\}$ . Within this paper we make always use of an admissible path  $\phi$ , i.e.  $\phi \in \Phi^{n,r}(\Lambda)$  and  $\int_\Lambda \|\phi(\lambda) - r\|^{n-1} d\lambda < \infty$ . This condition ensures that the X-ray transform

depending on an admissible path  $\phi$  which is defined for  $\lambda \in \Lambda$  und  $\theta \in S^{n-1}$  by  $\mathcal{D}_\phi f(\phi(\lambda), \theta) := \mathcal{D}_{\phi(\lambda)} f(\theta)$  turns into a continuous operator  $\mathcal{D}_\phi : L^2(\Omega_r^n) \rightarrow L^2(\Gamma_\phi \times S^{n-1})$ .

In [2] it was shown that a stable inversion of the X-ray transform can be performed if the path fulfills the so-called *Tuy conditions*, i.e.  $\phi \in \Phi^{n,r}(\Lambda)$  is bounded, continuous, differentiable a.e., and for all  $(x, \theta) \in \Omega_r^n \times S^{n-1}$  there exists an element  $\lambda \in \Lambda$  such that  $\langle x, \theta \rangle = \langle \phi(\lambda), \theta \rangle$  and  $\langle \phi'(\lambda), \theta \rangle \neq 0$ . Obviously, for the same  $\lambda \in \Lambda$  and all  $\rho \in \mathbb{R} \setminus \{0\}$  the equations  $\langle x, \rho\theta \rangle = \langle \phi(\lambda), \rho\theta \rangle$  and  $\langle \phi'(\lambda), \rho\theta \rangle \neq 0$  are also valid. Based on a Tuy path we define for  $\theta \in S^{n-1}$  and  $s \in \mathbb{R}$  the *Crofton symbol* by  $n_\phi(\theta, s) := \#\{\lambda \in \Lambda : \langle \phi(\lambda), \theta \rangle = s\}$ . For  $\rho \in \mathbb{R}$  we get immediately  $n_\phi(\rho\theta, \rho s) = n_\phi(\theta, s)$ . Using the Crofton symbol we define a function that is important for the inversion of the X-ray transform: Let  $\phi \in \Phi^{n,r}(\Lambda)$  be a Tuy path,  $\lambda \in \Lambda$  and  $y \in \Omega_r^n$ . We define

$$t_{\phi,\lambda,r}(y) := |\langle \phi'(\lambda), y \rangle| n_\phi(y, \langle \phi(\lambda), y \rangle)^{-1}.$$

The function  $t_{\phi,\lambda,r}$  is even and homogeneous of degree 1. Using the function  $t_{\phi,\lambda,r}$  we can formulate the following inversion formula for the X-ray transform.

**Theorem** Let  $\beta \in \mathbb{R}^+$  with  $\beta > \max\{1, n - 3/2\}$ ,  $f \in L^2(\Omega_r^n)$ ,  $\phi \in \Phi^{n,r}(\Lambda)$  a Tuy path with  $t_{\phi,\lambda,r} \in H^\beta(\Omega_r^n)$  for  $\lambda \in \Lambda$  and  $c_n := (2\pi)^{-n/2-1}$ . Then we have for almost every  $x \in \Omega_r^n$

$$(1) \quad f(x) = c_n \int_\Lambda \int_{S^{n-1}} \mathcal{D}_{\phi(\lambda)} f(\theta) \mathcal{G}_{\phi(\lambda)}^{n-2} \mathcal{T}_x \hat{t}_{\phi,\lambda,r}(\theta) d\theta d\lambda.$$

Using equation (1) we can derive reconstruction algorithms of filtered backprojection type. Depending on the number of approximations we achieve shift-variant or shift-invariant filtering. Based on equation (1) we can additionally derive an inversion formula for the extended X-ray transform which leads to a reconstruction algorithm of filtered layergram type. In this case no approximations are necessary. Details on all results of this contribution can be found in [7].

REFERENCES

[1] A. Kak and M. Slaney, *Principles of Computerized Tomographic Imaging*, IEEE Press (1998).  
 [2] H. K. Tuy, *An Inversion Formula for Cone-Beam Reconstruction*, SIAM Journal on Applied Mathematics **43(3)** (1983), 546–552.  
 [3] M. Defrise and R. Clack, *A Cone-Beam Reconstruction Algorithm using Shift-Variant Filtering and Cone-Beam Backprojection*, IEEE Transactions on Medical Imaging **13(1)** (1994), 186–195.  
 [4] H. Kudo and T. Saito, *Derivation and Implementation of a Cone-Beam Reconstruction Algorithm for Nonplanar Orbits*, IEEE Transactions on Medical Imaging **13(1)** (1994), 196–211.  
 [5] A. K. Louis, *Development of algorithms in computerized tomography*, in *The Radon Transform, Inverse Problems, and Tomography* (G. Olafsson and E. T. Quinto) (2006), 25–42.  
 [6] A. Katsevich, *An improved exact filtered backprojection algorithm for spiral computed tomography*, Advances in Applied Mathematics **32(4)** (2004), 681–697.

- [7] S. Oeckl, *Rekonstruktionsverfahren mit der Approximativen Inversen und einer neuen Formel zur Inversion der Röntgen-Transformation*, PhD thesis, Universität des Saarlandes, submitted.

## Thermoacoustics and the Spherical Radon Transform

S.K. PATCH

(joint work with MCW team)

Consider a spherical Radon transform

$$Rf(\mathbf{x}, t) = \int_{|x-y|=\nu_s t} f(y) dS_y$$

where  $\mathbf{x}$  represents the location of an ultrasound transducer,  $t$  is time, and  $\nu_s = 1.5\text{mm}/\mu\text{s}$  is propagation speed. Ultrasound reflection tomography motivated Norton and Linzer to derive series solutions for  $f$  for specific measurement geometries [1, 2, 3]. Concurrent experimental research on thermoacoustic phenomena neglected the mathematics of image reconstruction, although the idealized mathematical models were essentially identical [4, 5, 6, 8, 7]. Early thermoacoustic tomography systems reconstructed via filtered backprojection, applying the filter and weights of the standard (planar) Radon transform but accounting for the spherical integration surface during backprojection [9]. This approach causes low-frequency shading across the image volume, but was sufficiently accurate near the origin. Mathematically exact approaches to image reconstruction via filtered backprojection and also from a wide range of measurement geometries have been developed, primarily by members of the mathematical community. Image reconstruction is not currently a limiting factor in the development of thermoacoustic imaging. Understanding the thermoacoustic contrast mechanisms is required before thermoacoustic techniques can be translated into the clinic. For instance, just as xray CT projections are highly dependent upon the energy of the irradiating xrays, thermoacoustic signal production is as a function of irradiation frequency. Additionally, clinical ultrasound arrays rarely provide sufficient coverage to collect mathematically complete data. Finally, experimental constraints cause measured data to deviate from that modeled by the spherical Radon transform.

## REFERENCES

- [1] NORTON, S. 1980. *Reconstruction of a two-dimensional reflecting medium over a circular domain: exact solution*, Journal of the Acoustical Society of America, **67**, 1266-1273.
- [2] NORTON, S. and LINZER, M. 1979. *Ultrasonic Reflectivity Imaging in Three Dimensions: Reconstruction with Spherical Transducer Arrays*, Ultrasonic Imaging, **1**, 210-239.
- [3] NORTON, S. J. and LINZER, M. 1981. *Ultrasonic Reflectivity Imaging in Three Dimensions: Exact Inverse Scattering Solutions for Plane, Cylindrical, and Spherical Apertures*, IEEE Transactions on Biomedical Engineering, BME-**28**, 202-220.
- [4] BOWEN, T., NASONI, L., PIFER, A. E. and SEMBROSK, G. H. *Some Experimental Results on the Thermoacoustic Imaging of Tissue Equivalent Phantom Materials*. IEEE Ultrasonics Symposium 2. Chicago, IL, (1981).

- [5] CASPERS, F. and CONWAY, J. *Measurement of Power Density in a Lossy Material by means of Electromagnetically induced acoustic signals for non-invasive determination of spatial thermal absorption in connection with pulsed hyperthermia.* 12th European Microwave Conference Helsinki, (1982).
- [6] LIN, J. C. and CHAN, K. H. *Microwave Thermoelastic Tissue Imaging-System Design,* IEEE Transactions on Microwave Theory and Techniques, **32**, (1984), 854-860.
- [7] NASONI, R., LIEW, S., HALVERSON, P. and BOWEN, T. 1985. *Thermoacoustic Images Generated by a 2450 MHz Portable Source and Applicator.* IEEE Ultrasonics Symposium.
- [8] NASONI, R. L., EVANOFF, G. A., HALVERSON, P. G. and BOWEN, T. 1984. *Thermoacoustic Emission by Deeply Penetrating Microwave Radiation,* In: MCAVOY, B. R. (ed.) IEEE 1984 Ultrasonics Symposium. Dallas, TX.
- [9] KRUGER, R. A., LIU, P., FANG, Y. R. and APPLIEDORN, C. R. 1995. Photoacoustic ultrasound (PAUS) - Reconstruction Tomography. Medical Physics, **22**, 1605-1609.

### Inversion of the attenuated Radon transform via circular harmonics expansions and contours reconstruction

GAËL RIGAUD

(joint work with Aref Lakhali)

The attenuated Radon transform has been widely studied in the past decades due to its involvement in the modeling in medical imaging (SPECT) or physical imaging (Doppler tomography) [1]. This stimulating inverse problem were solved by Novikov in 2001 [2] and later by Natterer [3] in the non-uniform case. Before them, Tretiak and Metz [4] worked out a solution for a constant attenuation. We can also recall the recent work of Puro and Garin who have recently proposed in [5] an analytical inversion formula based on circular harmonic decomposition and for axially symmetric attenuation.

Chapman and Cary [6] studied the circular harmonic decomposition (CHD) of the classical (non attenuated in our context) Radon transform and showed the relevance of this approach. In particular, the induced image reconstruction algorithm presents similar results with the widely used filtered backprojection algorithm (FBP). The application of the CHD for SPECT data was also shown to be relevant in [7] which encourages the study of the attenuated Radon transform in circular harmonic space. A pioneering numerical algorithm based on this explicit inversion formula was derived and implemented in [8]. Akin to FBP, this algorithm uses Fourier space to implement the Riesz potential before to backproject.

As an alternative way, we propose to expand the reconstruction kernel of the attenuated Radon transform in circular harmonics to obtain a new reconstruction algorithm. In comparison with Kunyansky's algorithm [8] in which the inversion is proceeded in 2D-Fourier space, we use here an angular Fourier transform. From [3], we can deduce the reconstruction kernel of the attenuated Radon transform at a point  $x$

$$\Psi^x(p, \theta) = \frac{e^{h(p, \theta)}}{4\pi^2} \operatorname{div}_x \left[ \frac{\theta}{x \cdot \theta - p} e^{-u(x, \theta)} \right].$$

with  $u(x, \theta) = h(x \cdot \theta, \theta) - (\mathcal{D}a)(x, \theta^\perp)$  and

$$h(p, \theta) = \frac{1}{2} (\mathcal{I} + i\mathcal{H})(\mathcal{R}a)(p, \theta)$$

is the analytic representation of the signal  $\mathcal{R}a$  in which  $\mathcal{I}$ ,  $\mathcal{H}$  and  $\mathcal{D}$  are respectively the identity operator, the Hilbert transform and the Divergent beam transform. The induced reconstruction method can be understood as an extension of the Cormack's inversion formula [9] to the attenuated Radon transform without differentiation of the data. In addition the advantages of using the CHD remain and this new formulation may bring a new overview on the inversion of the attenuated Radon transform for further analytical investigations.

In addition, we propose to extract analytically the contours of the sought object from its attenuated Radon transform. Louis introduced in [10] a method to combine image reconstruction and image analysis. Using similar technique, we show the feasibility of this approach for such applications. Numerical results attest of the accuracy and stability of our method for image reconstruction and feature extraction.

#### REFERENCES

- [1] Natterer F and Wuebbeling F 2001 *Mathematical Methods in Image Reconstruction* (SIAM Monographs on Mathematical Modeling and Computation) (Philadelphia, PA: SIAM)
- [2] Novikov R 2002 An inversion formula for the attenuated X-ray transformation *Ark. Mat.*, **40** pp. 145-67.
- [3] Natterer F 2001 Inversion of the attenuated Radon transform *Inverse Problems* **17** 0266-5611
- [4] Tretiak O and Metz C 1980 The exponential Radon transform *SIAM J. Appl. Math.* **39** 341-54
- [5] Puro A and Garin A 2013 Cormack-type inversion of attenuated Radon transform *Inverse Problems* **29** 065004
- [6] Chapman C H and Cary P W, The circular harmonic Radon transform, *Inverse Problems*, vol. 2, pp. 23-49, 1986.
- [7] Hawkins W G, Lechner P K and Yang N C, The circular harmonic transform for SPECT reconstruction and boundary conditions on the Fourier transform of the sinogram *IEEE Transactions on Medical Imaging*, 7(2), pp 135-138, 1988.
- [8] Kunyansky L A 2001 A new SPECT reconstruction algorithm based on Novikov's explicit inversion formula *Inverse Problems* **17** 293-306
- [9] Cormack A M 1984 Radon's problem - old and new, *SIAM-AMS Proceedings* **14** pp. 33-39
- [10] Louis A K 2008 Combining Image Reconstruction and Image Analysis with an Application to 2D-Tomography *SIAM J Imaging Sciences* **01** 188-208

### Mathematics of STEM tomography

HOLGER KOHR

(joint work with T. Dahmen)

In HAADF-STEM (**H**igh **A**ngle **A**nnular **D**ark **F**ield **S**canning **T**ransmission **E**lectron **M**icroscopy), the imaging system consists of a *focused* electron beam which is moved across the specimen under investigation (scanning). This is in

contrast to conventional transmission electron microscopy where one single illumination of a sample yields an image showing absorption and diffraction contrast. In STEM imaging, the contrast mechanism is based on *incoherent scattering to high angles*. Since only these scattered electrons are noticed by the annular detector while the main beam does not contribute, one speaks of dark field imaging.

The most common mathematical model for STEM tomography has been the Radon transform since a very small opening angle of the electron beam allowed it to be well approximated by a ray. However, for thick specimens, blurring effects far from the focal plane are no longer negligible. Moreover, modern microscopes offer significantly larger beam opening angles, which makes it possible to acquire depth-resolved information about the specimen by varying the focal plane, thus acquiring a *focal series*, instead of performing rotations in order to apply tomography.

Recently, the two approaches were combined in the acquisition of a *tilt focal series*, and an ART-like iterative algorithm was implemented to compute reconstructions, however with a simplified adjoint operator not consistent with the forward model [2]. The talk introduced the measurement principle and the resulting convolution model

$$(1) \quad g(y) = p * f(y) = \int_{\mathbb{R}^3} p(y - x) f(x) dx, \quad y \in \mathbb{R}^3,$$

with the real-valued *probe function*  $p$  describing the spatial electron distribution of the beam during an illumination. Its actual form depends on the electron source size and directional distribution as well as some characteristic parameters of the optics which focus the beam [3]. Since this model is rotationally invariant, i.e.

$$p * f(R^{-1} \cdot) = p(R^{-1} \cdot) * f$$

for any rotation matrix  $R$ , it suffices to investigate the case when  $p$  describes a beam aligned with the  $x_3$  axis. In a simple approximation, it can be assumed that the electron density is uniform inside a double cone with opening semi-angle  $\alpha \in ]0, \pi/2[$ ,

$$C = \{x \in \mathbb{R}^3 \mid |x'| < \tan \alpha |x_3|\}, \quad x' = (x_1, x_2).$$

The corresponding probe function is given by

$$(2) \quad p(x) = \frac{1}{\pi \tan^2 \alpha x_3^2} \cdot \begin{cases} 1, & \text{if } |x'| < \tan \alpha |x_3|, \\ 0, & \text{otherwise,} \end{cases}$$

where the normalization factor ensures that physically, the total flux through each lateral cut of the cone is constant for each value of  $x_3$ .

Due to the simple convolution structure of the forward model, it is possible to deduce a Fourier slice theorem in order to gain insight into the frequency information about the unknown  $f$  contained in the data  $g$ . Since the connection is given by the classical formula  $\widehat{g} = (2\pi)^{3/2} \widehat{p} \cdot \widehat{f}$ , the shape and the support of  $\widehat{p}$  determine

the frequency content of  $g$ . Performing first the 2D Fourier transform with respect to  $(x_1, x_2)$ , one acquires

$$\begin{aligned} 2\pi \mathcal{F}_2 p(\xi', x_3) &= (\pi \tan^2 \alpha x_3^2)^{-1} \int_{|x'| < \tan \alpha |x_3|} e^{-i\langle \xi', x' \rangle} dx' \\ &= 2 \frac{J_1(\tan \alpha |x_3| |\xi'|)}{\tan \alpha |x_3| |\xi'|} \end{aligned}$$

with  $J_1$  being the Bessel function of the first kind with index 1. The remaining FT can now be computed to

$$\begin{aligned} (2\pi)^{3/2} \hat{p} &= 2 \int_{\mathbb{R}} \frac{J_1(\tan \alpha |x_3| |\xi'|)}{\tan \alpha |x_3| |\xi'|} e^{i\xi_3 x_3} dx_3 \\ &= \frac{4}{\tan \alpha |\xi'|} \int_0^\infty \frac{J_1(t)}{t} e^{-it \frac{\xi_3}{\tan \alpha |\xi'|}} dt \\ &= \frac{4}{\tan \alpha |\xi'|} \cdot \begin{cases} \sqrt{1 - \frac{\xi_3^2}{\tan^2 \alpha |\xi'|^2}}, & \text{if } \tan \alpha |\xi'| > |\xi_3|, \\ 0, & \text{otherwise,} \end{cases} \end{aligned}$$

where the last step makes use of [1, Formula (11.4.25)]. This formula has some interesting consequences due to the fact that  $\hat{p}$  is supported in the complement of a cone with opening angle  $\pi/2 - \alpha$ . Firstly,  $f$  can be uniquely recovered by a tilt series using equidistant angles with a step of less than  $\alpha$ . Secondly, the resolution along the beam is bad since the extent of the support in that direction is very small under practical conditions. Thirdly, however, in a combined tilt and focal series, the sampling distance of the focal planes can be chosen much larger than in the lateral direction, which makes it more attractive for practical scenarios.

#### REFERENCES

- [1] M. Abramowitz and I. A. Stegun. *Handbook of Mathematical Functions with Formulas, Graphs, and Mathematical Tables*. Dover, ninth dover printing, tenth gpo printing edition, 1972.
- [2] T. Dahmen, J.-P. Baudoin, A. R. Lupini, C. Kübel, P. Slusallek, and N. de Jonge. Combined Scanning Transmission Electron Microscopy Tilt- and Focal Series. *Microscopy and Microanalysis*, 20:548–560, 4 2014.
- [3] V. Intaraprasong, H. L. Xin, and D. A. Muller. Analytic derivation of optimal imaging conditions for incoherent imaging in aberration-corrected electron microscopes. *Ultramicroscopy*, 108(11):1454–1466, 2008.

**Methods for accelerating x-ray tomographic reconstruction**

MING JIANG

(joint work with Jason Cong, Yijin Guan, Peng Li, Guojie Luo, Peter Maaß,  
Thomas Page, Li Shen, Pei Wang, Peng Zhang, Wentai Zhang)

In addition to multi-CPU clusters, GPU and DSP, FPGA (field-programmable gate array) is another hardware accelerating approach. High-level synthesis tools from C to FPGA can optimize the implementation under the performance, power, and cost constraints, and enable energy-efficient accelerator-rich architecture. In previous work, we used FPGA for the simultaneous image reconstruction and segmentation with Mumford-shah regularization for XCT under  $\ell_1$ -convergence, and achieved 31X speed-up and 622X energy efficiency compared to CPU implementation [5, 8]. However, FGPA was only used to accelerate the computation of forward and backward projections. In this talk, we are reporting algorithmic development to accelerate the reconstruction further.

Because of the limited memory on chip, we proposed to use a combination of order-subset and coordinate decent methods to formulate our algorithms so that only small and necessary data are moved between the main memory and FPGA, so that the communication expense between CPU and FPGA can be reduced. The ordered-subset method, is also called the block-iterative method, and the online learning method in machine learning, and can be derived by the incremental gradient method in optimization theory [6, 4]. Assume that the reconstruction functional is of the following form

$$(1) \quad f(x) = \sum_{j=1}^M f_j(x).$$

At one iteration,  $f_j$  is chosen to update the image and the current image block under update is  $x_i$ . Then an update of the image block  $x_i$  by the incremental gradient descent method is

$$(2) \quad x_i \leftarrow x_i - \lambda \nabla_{x_i} f_j(x).$$

For XCT, each image block is naturally specified by the pixels intersected by one beam. For XCT, after applying the above scheme (2) to  $f$ , either the least-squares functional or the Kullback-Leibler divergence, we obtain the Kaczmarz method (also called the algebraic reconstruction techniques (ART)) or the row-action of the RAMLA method [7, 3, 1], respectively.

We propose to implement as many numbers of such algorithm blocks as possible in FPGA in an accelerator-rich architecture. Although algorithms in the above formulations (2) are sequential, they can also run in parallel with asynchronous updates to improve speed-up. Based on the previous results on block-iterative methods and asynchronous incremental gradient methods [2, 10, 6, 4], we expect the convergence of the proposed asynchronous parallel Kaczmarz (ART) and RAMLA methods with diminishing relaxations. Preliminary results demonstrate better early reconstruction images with both the asynchronous parallel Kaczmarz

(ART) and RAMLA methods with diminishing relaxations, than their conventional sequential versions.

After the talk at Oberwolfach, the speaker was kindly informed the work in [11, 9] by Prof. Stephen J. Wright of University of Wisconsin. The asynchronous parallel Kaczmarz method has been studied from the perspective of machine learning. The convergence of the asynchronous parallel Kaczmarz method has been established in the consistent case with constant relaxations in [9], together with extensions to inconsistent cases.

The proposed asynchronous parallel scheme fits well with the architecture of FPGA and reduces the communication cost, and is applicable to other parallel architectures in general (e.g. multi-core CPUs). In this talk, we also discuss more general asynchronous parallel data-block and image-block iterative methods with regularization similar to (1) and (2), and approaches to establish their convergence.

This work is supported in part by National Basic Research and Development Program of China (2011CB809105), and National Science Foundation of China (61121002).

#### REFERENCES

- [1] J. Browne and A. R. De Pierro. A row-action alternative to the EM algorithm for maximizing likelihood in emission tomography. *IEEE Transactions on Medical Imaging*, 15(5):687 – 699, 1996.
- [2] Dimitri P. Bertsekas and John N. Tsitsiklis. *Parallel and distributed computation: numerical methods*. Prentice Hall, Englewood Cliffs, N.J., 1989.
- [3] R. Gordon, R. Bender, and G. T. Herman. Algebraic reconstruction techniques (ART) for three-dimensional electron microscopy and x-ray photography. *Journal of Theoretical Biology*, 29:471 – 482, 1970.
- [4] M. Jiang. Iterative algorithms for image reconstruction. In C. Leondes, editor, *Medical Imaging Systems: Technology and Applications*, volume I, pages 351 – 382, Singapore, 2005. World Scientific.
- [5] M. Jiang, P. Maass, and T. Page. Regularizing properties of the mumford-shah functional for imaging applications. *Inverse Problems*, 30, 2014.
- [6] M. Jiang and G. Wang. Convergence studies on iterative algorithms for image reconstruction. *IEEE Transactions on Medical Imaging*, 22(5):569 – 579, 2003.
- [7] S. Kaczmarz. Angenäherte auflösung von systemn linearer gleichungen. *Bulletin International de l'Academie Polonaise des Sciences et Lettres*, 35:355 – 357, 1937.
- [8] Peng Li, Thomas Page, Guojie Luo, Wentai Zhang, Pei Wang, Peng Zhang, Peter Maass, Ming Jiang, and Jason Cong. Fpga acceleration for simultaneous medical image reconstruction and segmentation. In *Field-Programmable Custom Computing Machines (FCCM), 2014 IEEE 22nd Annual International Symposium on*, pages 172–172.
- [9] Ji Liu, Stephen J. Wright, and Srikrishna Sridhar. An asynchronous parallel randomized kaczmarz algorithm. preprint, 2014.
- [10] A. Nedić, D. P. Bertsekas, and V. S. Borkar. *Distributed asynchronous incremental subgradient methods*, volume Volume 8, pages 381–407. Elsevier, 2001.
- [11] Feng Niu, Benjamin Recht, Christopher Ré, and Stephen J. Wright. Hogwild: A lock-free approach to parallelizing stochastic gradient descent. In J. Shawe-taylor, R.s. Zemel, P. Bartlett, F.c.n. Pereira, and K.q. Weinberger, editors, *Advances in Neural Information Processing Systems 24*, pages 693–701. 2011.

## Acousto-Optic Inverse Source Problem

JOHN C. SCHOTLAND

(joint work with Guillaume Bal)

The development of tools for molecular imaging has had a transformative effect on biomedical research [1]. There are multiple applications including mapping gene expression and following the course of infection in a single animal, among others. Optical methods hold great promise for molecular imaging, due to their spectroscopic sensitivity to chemical composition, nondestructive nature and relatively low cost [2]. One particularly popular modality, known as bioluminescence imaging, makes use of a bioluminescent marker, most often the luciferin-luciferase system, as a reporter of molecular activity [3, 4]. In a typical experiment, genetically modified light-emitting cells are introduced into a model organism and a CCD camera is used to record the intensity of emitted light. The resulting images convey information about the spatial distribution of the labeled cells. However, the images are not tomographic nor are they quantitatively related to the number density of the cells. One approach to this problem is to reconstruct the number density (optical source) from measurements of multiply-scattered light, a method known as bioluminescence tomography (BLT) [5, 6, 7, 8, 9, 10, 12, 11, 13]. The corresponding inverse problem is a classical inverse source problem (ISP) and it is well known that such problems do not have unique solutions [14]. That is, more than one source can give rise to the same measurements. Uniqueness can be restored under strong mathematical assumptions, requiring *a priori* knowledge of the source geometry.

To overcome the problem of non uniqueness in BLT requires a fundamentally new approach. In this work, we propose a novel imaging modality termed ultrasound modulated bioluminescence tomography (UMBLT), which is in the spirit of several recently developed hybrid imaging methods. In hybrid imaging (also called multi-wave imaging), an external field is used to control the material properties of a medium of interest, which is then probed by a second field [15, 16, 17, 19, 18, 20, 22, 23, 24, 25, 26, 27, 28, 29, 30, 31]. In the physical setting we consider, the source density is spatially modulated by an acoustic wave, while measurements of the emitted light are recorded. We find that it is possible to *uniquely* reconstruct the source density by an algebraic formula. Moreover, the reconstruction is stable in the sense that an error in the measurements is linearly related to the error in recovering the source. We note that the inverse problem of UMBLT has a quite different mathematical structure than those that arise in other hybrid imaging modalities such as acousto-optic tomography (AOT) [18]. In particular, the inverse problem of AOT is an inverse scattering problem which consists of solving a *nonlinear* partial differential equation. In contrast, the inverse problem of UMBLT is an inverse source problem which is formulated as a *linear* partial differential equation.

## REFERENCES

- [1] R. Weissleder and U. Mahmood, *Radiology* **219**, 316–333 (2001).
- [2] V. Ntziachristos, J. Ripoll, L. H. V. Wang, and R. Weissleder, *Nat. Biotech.* **23**, 313–320 (2005).
- [3] C. Contag and M. H. Bachmann, *Annu. Rev. Biomed. Eng.* **4**, 235–260 (2002).
- [4] A. McCaffrey, M. A. Kay and C. H. Contag, *Molecular Imaging* **2**, 75–86 (2003).
- [5] G. Wang, E. A. Hoffman, G. McLennan, L. V. Wang, M. Suter and J. Meinel, *Radiology* **229(P)**, 566 (2003).
- [6] G. Wang, Y. Li and M. Jiang, *Med. Phys.* **31**, 2289–2299 (2004).
- [7] X. Gu, Q. Zhang, L. Larcom and H. Jiang, *Opt. Express* **12**, 3996–4000 (2004).
- [8] W. Cong et al. *Optics Express* **13**, 6756–6771 (2005).
- [9] Ming Jiang, Tie Zhou, Jiantao Cheng, Wenxiang Cong and Ge Wang, *Optics Express* **15** 11095–11116 (2007).
- [10] S. Ahn, A.J. Chaudhari, F. Darvas, C.A. Bouman and R.M. Leahy, *Phys. Med. Biol.* **53**, 3921–3942 (2008).
- [11] Y. Lu, X. Zhang, A. Douraghy, D. Stout, J. Tian, T. F. Chan and A. F. Chatziioannou, *Opt. Express* **17**, 8062–8080 (2009).
- [12] H. Dehghani, S. C. Davis and B. W. Pogue, *Med. Phys.* **35**, 4863–4871 (2008).
- [13] S. Shi and H. Mao, *Biomedical Optics Express* **4**, 709–724 (2013).
- [14] V. Isakov, *Inverse Source Problems* (American Mathematical Society, Providence, 1990).
- [15] L. H. Wang (Editor), *Photoacoustic imaging and spectroscopy* (CRC Press, 2009).
- [16] H. Ammari, E. Bonnetier, Y. Capdeboscq, M. Tanter and M. Fink, *SIAM J. Appl. Math.* **68**, 1557–1573 (2008).
- [17] Y. Capdeboscq, J. Fehrenbach, F. de Gournay and O. Kavian, *SIAM J. Imaging Sciences*, **2**, 1003–1030 (2009).
- [18] G. Bal and J. C. Schotland, *Phys. Rev. Lett.* **104**, 043902 (2010).
- [19] G. Bal in *Inside Out II*, G. Uhlmann Editor (Cambridge University Press, Cambridge, UK, 2012).
- [20] G. Bal and G. Uhlmann, *Comm. Pure Appl. Math.* **66**, 1629–1652 (2013).
- [21] G. Bal, *Contemporary Mathematics* (in press).
- [22] G. Bal, E. Bonnetier, F. Monard and F. Triki, *Inverse Problems and Imaging* **7**, 353–375 (2013).
- [23] G. Bal, W. Naetar, O. Scherzer and J. Schotland, *J. Ill-Posed and Inverse Problems* **21**, 265280 (2013).
- [24] B. T. Cox, S. R. Arridge and P. C. Beard, *J. Opt. Soc. Am. A*, **26**, 443–455 (2009).
- [25] B. Gebauer and O. Scherzer, *SIAM J. Applied Math.* **69**, 565–576 (2009).
- [26] P. Kuchment and L. Kunyansky, *J. Appl. Math.* **19**, 191–224 (2008); *ibid Inverse Problems* **27** 055013 (2011).
- [27] P. Kuchment and D. Steinhauer, *Inverse Problems* **28**, 084007 (2012).
- [28] F. Monard and G. Bal, *Inverse Problems and Imaging* **6**, 289–313 (2012).
- [29] J. R. McLaughlin and J. Yoon, *Inverse Problems* **20**, 2545 (2004).
- [30] J. R. McLaughlin, N. Zhang and A. Manduca, *Inverse Problems* **26**, 085007 (2010).
- [31] Adrian Nachman, Alexandru Tamaskan and Alexandre Timonov, *Inverse Problems* **23**, 2551–2563 (2007); *ibid, Inverse Problems* **25**, 035014 (2009).

### Regularisation Methods for Joint Image Reconstruction

SIMON ARRIDGE

(joint work with Matthias J. Ehrhardt)

Combining images of the same object from several different instruments has been a widely studied problem, and is often approached as a task in *data fusion*, for example involving the determination of an unknown transformation that registers two or more images acquired in different coordinate systems, so that common structures may be visualised. In contrast to this, fully multimodal systems are becoming increasingly prevalent in medical imaging, including commercial systems based on PET-CT, SPECT-CT and MRI-PET, amongst others[1, 2]. These systems acquire data simultaneously, and suggest that the corresponding problem to be studied is one of *joint image reconstruction*.

Considering the case of two images  $u, v$  we define the forward model

$$\begin{pmatrix} A^{(u)} \\ A^{(v)} \end{pmatrix} : \begin{pmatrix} u \\ v \end{pmatrix} \mapsto \begin{pmatrix} g^{(u)} \\ g^{(v)} \end{pmatrix},$$

and the corresponding data fit terms

$$\ell(g^{(u)}, A^{(u)}(u)) = -\log P(g^{(u)}|u); \quad \ell(g^{(v)}, A^{(v)}(v)) = -\log P(g^{(v)}|v)$$

where each of the mappings  $A^{(u)}, A^{(v)}$  may be separately either well-posed or weakly or strongly illposed, and either linear or non-linear. If we assume that the noise models of each modality are uncorrelated then the reconstructed images will also be uncorrelated except through the involvement of a coupled image prior model  $\pi(u, v)$  and the corresponding regularisation functional  $\Psi = -\log \pi$ . Two different cases can be defined :

- “One-sided” reconstruction assumes that  $A^{(v)}$  is well posed and that the image  $v_*$  is stably reconstructed and used as a fixed auxiliary image to influence the reconstruction of  $u$ , through the conditional prior  $\Psi(u|v_*) = -\log \pi(u|v_*)$ . In the Bayesian framework this leads to a minimisation problem for the Maximum a Posteriori (MAP) estimate :

$$u_* = \min_u \left[ -\log P(u|g^{(u)}, v_*) := \ell(g^{(u)}, A^{(u)}(u)) + \Psi(u|v_*) \right]$$

- Joint reconstruction which optimises for both images simultaneously to give the Joint Maximum a Posteriori (JMAP) estimate:

$$\begin{pmatrix} u_* \\ v_* \end{pmatrix} = \min_{u,v} \left[ -\log P(u, v|g^{(u)}, g^{(v)}) := \ell(g^{(u)}, A^{(u)}(u)) + \ell(g^{(v)}, A^{(v)}(v)) + \Psi(u, v) \right]$$

Two contrasting approaches to defining the joint prior  $\pi(u, v)$  or conditional prior  $\pi(u|v)$  can be identified. The first uses a statistical similarity such as joint entropy [3]

$$\pi(u, v) = \exp \left[ \int_{\Omega(u)} \int_{\Omega(v)} P(u, v) \log(P(u, v)) dx_u dx_v \right]$$

which favours joint images with the minimum number of classes and the minimum within-class variance, and is closely related to the corresponding optimisation problem used in many image registration problems. The second approach defines a prior which favours joint structural similarity and/or joint sparsity. In our approach we consider a model which we call *Parallel Level Sets* [4] and define a functional of the form

$$\Psi(u, v) = \int_{\Omega} \varphi \left( \psi (\|\nabla u\| \|\nabla v\|) - \psi (\|\langle \nabla u, \nabla v \rangle\|) \right)$$

where  $\varphi, \psi : [0, \infty) \rightarrow \mathbb{R}$  are strictly increasing and  $\varphi(0) = 0$ . Minimisation of this functional leads to an image flow of the form

$$\begin{aligned} \frac{\partial u}{\partial t} &= \nabla \cdot (R[v]\Lambda[u, v]R[v]^T \nabla u) \\ \frac{\partial v}{\partial t} &= \nabla \cdot (R[u]\Lambda[v, u]R[u]^T \nabla v) \end{aligned}$$

where  $R[u], R[v]$  are rotation matrices defining local gauge coordinates normal and parallel to the level sets of  $u, v$  respectively, and  $\Lambda[u, v] = \text{diag}(\gamma^{\perp}(u, v), \gamma^{\parallel}(u, v))$  defines the anisotropy of flow in the normal and tangential directions.

Different image flow behaviour results from different choices of  $\phi$  and  $\psi$ . A desirable form would be one that becomes isotropic in the absence of gradients in either image, and becomes edge-enhancing for strong gradients, whilst being unbiased in the case that structure is absent in either image separately. In [5], results have been shown for a model of MRI-PET, with underampled k-space for MRI and partial volume and Poisson statistics for PET. It was found that the joint regularisation improves over other approaches such as joint-TV.

#### REFERENCES

- [1] S.R. Cherry, *Multimodality in Vivo Imaging Systems: Twice the Power or Double the Trouble?*, Annual Review of Biomedical Engineering, **8**, (2006), 35-62.
- [2] D.W. Townsend, *Multimodality Imaging of Structure and Function*, Physics in Medicine and Biology, **53**(4), (2008), R1-R39.
- [3] S. Somayajula, C. Panagiotou, A. Rangarajan, Q. Li, S.R. Arridge, and R.M. Leahy. *PET Image Reconstruction Using Information Theoretic Anatomical Prior*. IEEE Transactions on Medical Imaging, **30**(3), (2011), 537-549.
- [4] M.J. Ehrhardt and S.R. Arridge, *Vector-Valued Image Processing by Parallel Level Sets*, IEEE Transactions on Image Processing, **23**(1), (2014), 9-18.
- [5] M.J. Ehrhardt, K. Thielemans, L. Pizarro, D. Atkinson, S. Ourselin, B. Hutton and S.R. Arridge, *Joint Reconstruction of PET-MRI by Exploiting Structural Similarity*, Inverse Problems, (In press, 2014).
- [6] L.A. Gallardo and M.A. Meju, *Characterization of Heterogeneous Near-Surface Materials by Joint 2D Inversion of DC Resistivity and Seismic Data*, Geophysical Research Letters, **30**(13), (2003), 1658.
- [7] E. Haber and M. Holtzman-Gazit, *Model Fusion and Joint Inversion*, Surveys in Geophysics, **34**, (2013), 675-695.
- [8] N. Sochen, R. Kimmel and R. Malladi. *A General Framework for Low Level Vision*, IEEE Transactions on Image Processing, **7**(3), (1998), 310-318.
- [9] J.P. Kaipio, V. Kolehmainen, M. Vauhkonen and E. Somersalo. *Inverse Problems with Structural Prior Information*, Inverse Problems, **15**, (1999), 713-729.

**On an exact inversion formula for 3D cone beam vector tomography**

THOMAS SCHUSTER

(joint work with Alexander Katsevich)

Cone beam vector tomography means the determination of a 3D vector field  $\mathbf{f}(x)$  from integral data that are acquired from ultrasound measurements. E.g. such a vector field is the velocity field of a moving fluid inside a bounded domain  $\Omega \subset \mathbb{R}^3$ . The data are accomplished by either measuring the time-of-flight or the Doppler spectral shift, both of which yield the integral of  $\mathbf{f}$  along the path of the ultrasound beam probed by its tangential direction. In case of a homogeneous medium the ultrasound beams propagate as lines and the mathematical model hence is described by the cone beam transform

$$(1) \quad [\mathbf{Df}](y(s), \Theta) = \int_0^\infty \mathbf{f}(y(s) + t\Theta) \cdot \Theta \, dt.$$

Here  $y(s)$ ,  $s \in \Lambda \subset \mathbb{R}$ , denotes the parametrization of a source trajectory  $\Gamma \subset (\mathbb{R}^3 \setminus \overline{B^3})$  and  $\Theta \in S^2 := \{x \in \mathbb{R}^3 : |x| = 1\} = \partial B^3$  is the unit vector along the ray that emanates from the source  $y(s)$ . It is assumed that  $\Theta \in \mathcal{C}$ , where  $\mathcal{C}$  is a cone and that  $B^3 \subset y(s) + \mathcal{C}$ , i.e. the unit ball is completely contained inside the union of the rays emanating from any source position  $y(s)$ . It is obvious that any potential field  $\mathbf{f} = \nabla v$  with potential  $v \in H_0^1(\Omega)$  is in the null space of  $\mathbf{D}$  and thusly only solenoidal vector fields can be reconstructed.

In the talk we present an inversion formula for  $\mathbf{D}$  which is exact for smooth, divergence free vector fields  $\mathbf{f}$ , i.e.  $\nabla \cdot \mathbf{f} = 0$ . A key role plays a Grangeat-like formula which has been proven by Kazantsev and Schuster in [3] and which relies on a splitting of the Radon transform

$$[\mathbf{Rf}](p, \eta) = \int_{x \cdot \eta = p} \mathbf{f}(x) \, dx$$

into its normal part

$$[\mathbf{R}^{(nor)}\mathbf{f}](p, \eta) := (\eta \cdot [\mathbf{Rf}](p, \eta))\eta, \quad p \in [-1, 1], \eta \in S^2$$

and its tangential part

$$[\mathbf{R}^{(tan)}\mathbf{f}](p, \eta) := [\mathbf{Rf}](s, \eta) - [\mathbf{R}^{(nor)}\mathbf{f}](p, \eta).$$

This formula reads as (compare [3, Theorem 5.1])

$$(2) \quad - \int_{S^2} [\mathbf{D}^{(even)}\mathbf{f}](x, \Theta) \delta''(\eta \cdot \Theta) \, d\Theta = \left( \operatorname{div}_\eta [\mathbf{R}^{(tan)}\mathbf{f}](p, \eta) \right) \Big|_{p=\eta \cdot x} + x \cdot \frac{\partial}{\partial p} [\mathbf{R}^{(tan)}\mathbf{f}](p, \eta) \Big|_{p=\eta \cdot x}.$$

Here  $\mathbf{D}^{(even)}\mathbf{f}$  means the even part of the measure data,

$$[\mathbf{D}^{(even)}\mathbf{f}](y(s), \Theta) = \frac{[\mathbf{Df}](y(s), \Theta) + [\mathbf{Df}](y(s), -\Theta)}{2}$$

and  $\operatorname{div}_\eta$  is the operator of surface divergence. In [3] the authors could prove that, if  $\Gamma$  satisfies a Tuy condition of order 3, which means that any plane passing through  $B^3$  intersects  $\Gamma$  in at least 3 points which are not located on a line, then a solenoidal vector field can be completely recovered from (1) using formula (2). The reconstruction is done in two steps:

- (1) Compute  $\mathbf{R}^{(tan)}\mathbf{f}$  with the help of eq. (2) using Tuy's condition of order 3.
- (2) Determine  $\mathbf{R}^{(nor)}\mathbf{f}$  from  $\mathbf{R}^{(tan)}\mathbf{f}$  using an expansion with respect to vector spherical harmonics.

We note that step (2) is only possible for solenoidal  $\mathbf{f}$ .

To deduce an exact inversion formula, that means a formula which avoids any series expansions, we hold on this scheme and use arguments from [1] where the author obtained an inversion formula for the scalar cone beam transform. Consequently our inversion formula consists of two parts,  $\mathbf{f}_1$ ,  $\mathbf{f}_2$ . The main result is subsumed in the following theorem.

**Theorem 1:** Let  $\mathbf{f}^s \in H(\operatorname{div}; B^3)$  be the projection of a  $C_0^\infty(B^3)$ -vector field  $\mathbf{f}$  onto the solenoidal vector fields, and  $\Gamma$  satisfy Tuy's condition of order 3. Then

$$\mathbf{f}^s = \mathbf{f}_1 + \mathbf{f}_2$$

with

$$\begin{aligned} \mathbf{f}_1(x) &= \frac{1}{8\pi^2} \int_\Lambda \frac{1}{|x-y(s)|} \int_0^{2\pi} [\Phi_{\theta\theta}(s, \alpha(\theta)) + \Phi(s, \alpha(\theta))] \\ &\quad \times \int_0^{2\pi} \frac{g(y(s), \cos \gamma \alpha^\perp(\theta) + \sin \gamma \beta(s, x))}{\cos^2 \gamma} d\gamma d\theta ds, \\ \mathbf{f}_2(x) &= - \int_{S^2} \alpha \int_{S^2} \sum_{\tilde{s}_j \in \tilde{\mathcal{S}}} \phi(\tilde{s}_j, \tilde{\mathcal{S}}) G(\tilde{s}_j, \eta) \cdot \nabla_\eta K(\alpha \cdot \eta) d\eta d\alpha, \end{aligned}$$

where  $\beta(s, x) = (x - y(s))/|x - y(s)|$ ,  $\alpha(\theta) \in (S^2 \cap \beta^\perp)$  for  $\theta \in [0, 2\pi)$ ,  $\alpha^\perp(\theta) = \alpha(\theta) \wedge \beta$ ,  $\tilde{\mathcal{S}} = \tilde{\mathcal{S}}(x \cdot \alpha, \eta)$  is any nondegenerate triple of points obtained by solving

$$y(\tilde{s}) \cdot \eta = x \cdot \alpha,$$

$g = \mathbf{D}^{(even)}\mathbf{f}$  is the even part of the cone beam transform of  $\mathbf{f}$ ,

$$G(s, \alpha) = - \int_{S^2} g(y(s), \Theta) \delta''(\Theta \cdot \alpha) d\Theta,$$

$$4\pi K(t) = \sqrt{\frac{2}{1-t}} - \ln\left(1 + \sqrt{(1-t)/2}\right) + \frac{1}{2} \ln((1-t)/2) - 1,$$

and  $\phi$ ,  $\Phi$  are certain, known functions defined on  $\Lambda \times S^2$  and depending solely on  $\Gamma$ .

Details of the proof are outlined in [2]. Figure 1 shows a numerical reconstruction using Theorem 1 of the solenoidal vector field  $\mathbf{f}(x) = \text{curl}(h_r(x)\mathbf{F}(x))$  with  $\mathbf{F}(x) = (0, 0, x_1 + x_2)$  and a cut-off function  $h_r$  which is compactly supported in  $B_r(0)$  with  $r = 1.95$ .

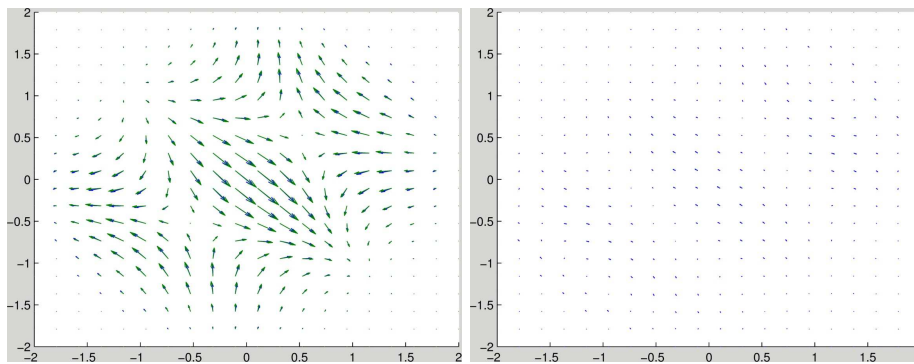


FIGURE 1. Exact and reconstructed field (left picture) using 50 sources and  $22 \times 22$  detector elements; error (right picture). The plots show the  $x - y$ -plane.

#### REFERENCES

- [1] A. Katsevich, *A general scheme for constructing inversion algorithms for cone beam CT*, Int. J. Math. Sci. **21** (2003), 1305–1321.
- [2] A. Katsevich and T. Schuster, *An exact inversion formula for cone beam vector tomography*, Inverse Problems **29** (2013), 13pp.
- [3] S.G. Kazantsev and T. Schuster, *Asymptotic inversion formulas in 3D vector field tomography for different geometries*, J. Inverse Ill-Posed Problems **19** (2011), 769–799.

#### Contrast-enhanced and sparse reconstruction for sub-sampled MR velocity imaging

CAROLA-BIBIANE SCHÖNLIEB

(joint work with Martin Benning, Lynn Gladden, Daniel Holland, Andy Sederman, Tuomo Valkonen)

In Phase-encoded Magnetic Resonance (MR) velocity imaging the inverse problem is the retrieval of the velocity of a fluid (or gas) from Fourier measurements. Here, the velocity is computed as the difference of the phases of complex signals encoded in MR measurements at two consecutive times. It is used widely. In medical imaging, it is used to study the distribution and variation in flow in blood vessels and around the heart to both diagnose and understand congenital heart disease and the behaviour of heart valves [1]. In the physical sciences, MR velocity imaging has been used to study the rheology of complex fluids [2], liquids and

gases flowing through packed beds [3, 4, 5], granular flows [6, 7] and multiphase turbulence [8]. The main advantage of MR for studying flow is that it is possible to non-invasively image systems without the use of a tracer. However, a major drawback of the technique, in both medical and non-medical applications, is the acquisition time of the measurement. In the medical field, long acquisition times ( $\sim$ min) necessitate breath hold or triggered acquisition techniques that, although impressive, are susceptible to artefacts and may be impractical in certain cases. In non-medical applications, long acquisition times require very stable systems and can prohibit the study of certain features, e.g. fine vortices in turbulent flow. To overcome these limitations many studies have explored methods to increase the temporal resolution of velocity-encoded imaging (e.g. [9, 10, 11]). These ultra-fast ( $\leq 1$  s imaging time) techniques have all been demonstrated to provide a substantial improvement in the temporal resolution. However, despite these advances, each has limitations in terms of the systems that can be studied and the trade-off between spatial and temporal resolution. In this talk we discuss two variational regularisation approaches which can both improve upon the spatial resolution of reconstructions from sub-sampled k-space data. Both methods are based on the theory of compressed sensing, exploiting prior knowledge of the signal or the velocity in terms of appropriate variational regularisation techniques. The first method is discussed in [12]. It constitutes the solution of the linear inverse problem of reconstructing a complex signal from its MR measurements by variational regularisation, and computing the velocity as the difference of the phases of two so reconstructed signals. We are particularly interested in regularisers that correctly treat both smooth and geometric features of the image. These features are common to velocity imaging, where the flow field will be smooth but interfaces between the fluid and surrounding material will be sharp, but are challenging to represent sparsely. As an example we demonstrate the variational approaches on velocity imaging of water flowing through a packed bed of solid particles. We evaluate Wavelet regularisation against Total Variation and the relatively recent second order Total Generalised Variation regularisation. We combine these regularisation schemes with a contrast enhancement approach called Bregman iteration. We verify for a variety of sampling patterns that Morozov's discrepancy principle provides a good criterion for stopping the iterations. Therefore, given only the noise level, we present a robust guideline for setting up a variational reconstruction scheme for MR velocity imaging. The main disadvantage of this first approach is that prior knowledge in terms of regularisation is not formulated for the quantity of interest, the velocity. This is suboptimal, especially since the amplitude and phase of the complex image have very different regularity properties, the former being relatively smooth while the latter being better approximated by a piecewise constant function. Therefore, we investigate a second approach where we attempt to reconstruct the desired velocity (the difference of the phases) directly, cf. also [13]. This amounts to the solution of a nonlinear inverse problem in which the phase is nonlinearly (via the exponential function) related to the MR measurements. We again derive a variational regularisation model (this time the regularisation acts on

the velocity directly!) and employ for the solution of this – now nonlinear problem – simultaneously linearisation and ADMM iteration. In each iteration this results in the solution of an unconstrained linear problem which we further break down to pure proximity operations by a surrogate approach. First experiments with this approach promise improved reconstruction properties. The convergence of the resulting iterative scheme still has to be analysed in more detail.

## REFERENCES

- [1] P. Gatehouse, J. Keegan, L. Crowe, S. Masood, R. Mohiaddin, K.-F. Kreitner and D. Firmin, *Applications of phase-contrast flow and velocity imaging in cardiovascular MRI*, *European Radiology* **15** (2005), 2172–2184.
- [2] P. Callaghan, *Rheo-NMR: nuclear magnetic resonance and the rheology of complex fluids*, *Reports on Progress in Physics* **62** (1999), 599–670.
- [3] A. Sederman, M. Johns, P. Alexander and L. Gladden, *Structure-flow correlations in packed beds*, *Chemical engineering Science* **53** (1998), 2117–2128.
- [4] M. H. Sankey, D. J. Holland, L. F. Gladden and A. J. Sederman, *Magnetic resonance velocity imaging of liquid and gas two-phase flow in packed beds*, *Journal of Magnetic Resonance* **196** (2009), 142–148.
- [5] D. J. Holland, D. M. Malioutov, A. Blake, A. J. Sederman and L. F. Gladden, *Reducing data acquisition times in phase-encoded velocity imaging using compressed sensing*, *Journal of Magnetic Resonance* **203** (2010), 236–246.
- [6] E. Fukushima, *Nuclear magnetic resonance as a tool to study flow*, *Annual Review of Fluid Mechanics* **31** (1999), 95–123.
- [7] D. J. Holland, L. F. Gladden, C. R. Müller, J. S. Dennis and A. J. Sederman, *Spatially resolved measurement of anisotropic granular temperature in gas-fluidized beds*, *Powder Technology* **182** (2008), 171–181.
- [8] A. B. Tayler, D. J. Holland, A. J. Sederman and L. F. Gladden, *Exploring the origins of turbulence in multiphase flow using compressed sensing MRI*, *Physical Review Letters* **108** (2012), 264505.
- [9] K. Kose, *Instantaneous flow-distribution measurements of the equilibrium turbulent region in a circular pipe using ultrafast NMR imaging*, *Physical Review A* **44** (1991), 2495–2504.
- [10] A. J. Sederman, M. D. Mantle, C. Buckley and L. F. Gladden, *MRI technique for measurement of velocity vectors, acceleration, and autocorrelation functions in turbulent flow*, *Journal of Magnetic Resonance* **166** (2004), 182–189.
- [11] P. Galvosas and P. T. Callaghan, *Fast magnetic resonance imaging and velocimetry for liquids under high flow rates*, *Journal of Magnetic Resonance* **181** (2006), 119–125.
- [12] M. Benning, L. Gladden, D. Holland, C. Schönlieb, T. Valkonen, *Phase reconstruction from velocity-encoded MRI measurements – A survey of sparsity-promoting variational approaches*, *Journal of Magnetic Resonance* **238** (2014), 26–43.
- [13] F. Zhao, D.C. Noll, J.F. Nielsen, J.A. Fessler, *Separate magnitude and phase regularization via compressed sensing*, *Medical Imaging, IEEE Transactions on*, **31**(9), (2012), 1713–1723.

## Multi-resolution method for choosing the total variation regularization parameter in X-ray tomography

SAMULI SILTANEN

(joint work with Keijo Hämäläinen, Aki Kallonen, Ville Kolehmainen, Matti Lassas, Esa Niemi and Kati Niinimäki)

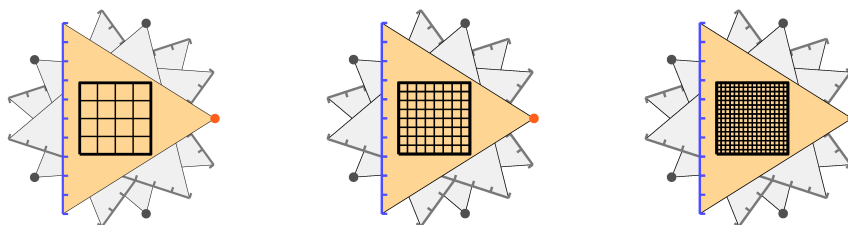
Consider the pencil-beam model  $m_0 = Af$  for X-ray tomography [3, Section V.4.1]. Here  $f \in \mathbb{R}^n$  is a discrete model of the unknown X-ray attenuation function, and  $m \in \mathbb{R}^k$  is the data vector. The inverse problem of tomography is to recover  $f$  approximately and stably from a noisy measurement  $m = Af + \varepsilon$ .

In total variation (TV) regularization one finds a regularized solution as the minimizer of this functional:

$$(1) \quad \|Af - m\|_2^2 + \alpha \|Lf\|_1,$$

where  $L$  is a discretization of a first-order differential operator and  $\alpha > 0$  is a regularization parameter. Choosing  $\alpha$  automatically is a challenging research problem; there are only a few suggested solutions in the literature [5, 1, 2]

In the schematic setup below we have 5 projection directions and a 10-pixel detector. Therefore, the number of data points is  $k = 50$ . The resolution of the discrete model can be freely chosen according to computational resources and other considerations. The number of degrees of freedom in the three discrete models below are  $n = 16$  and  $n = 64$  and  $n = 256$ , respectively.

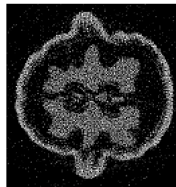


Our hypothesis is that if one solves the minimization problem (1) with the same data vector  $m$  but with several resolutions  $n$ , the resulting reconstructions should converge to a limit case as  $n \rightarrow \infty$ . We tested this hypothesis in [4] using tomographic data measured from a walnut.

TV reconstructions of a walnut at three resolutions using  $\alpha = 0.001$ :



$128 \times 128$

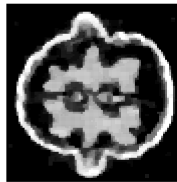


$192 \times 192$

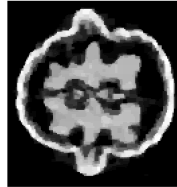


$256 \times 256$

TV reconstructions at three resolutions using a larger parameter  $\alpha = 10$ :



$128 \times 128$



$192 \times 192$



$256 \times 256$

As you can see in the above pictures, the smaller parameter leads to reconstructions that are unstable with respect to the resolution. On the other hand, using the larger parameter apparently gives converging reconstructions.

A systematic study of the same data with two noise levels suggests that it is reasonable to choose the smallest parameter  $\alpha > 0$  that leads to convergent reconstructions. Here is a table of TV norms of reconstructions (left: low noise, right: higher noise):

$\alpha$	$128^2$	$192^2$	$256^2$	$128^2$	$192^2$	$256^2$
$10^{-4}$	1.51	2.29	3.64	2.42	5.05	8.71
$10^{-3}$	1.51	2.29	3.46	2.43	5.05	8.59
$10^{-2}$	1.50	2.23	2.97	2.42	5.01	8.59
$10^{-1}$	1.43	1.85	1.93	2.37	4.83	8.16
$10^0$	1.08	1.11	1.11	1.99	3.50	5.12
$10^1$	0.78	0.78	0.77	0.86	0.86	0.88
$10^2$	0.48	0.48	0.48	0.48	0.48	0.48
$10^3$	0.12	0.12	0.12	0.12	0.12	0.12
$10^4$	0.04	0.04	0.04	0.04	0.04	0.04
$10^5$	0	0	0	0	0	0
$10^6$	0	0	0	0	0	0

Careful study of the above numbers suggests choosing  $\alpha = 1$  for the low-noise case and  $\alpha = 10$  for the high-noise case.

#### REFERENCES

- [1] K. HÄMÄLÄINEN, A. KALLONEN, V. KOLEHMAINEN, M. LASSAS, K. NIINIMÄKI, AND S. SILTANEN, *Sparse tomography*, SIAM Journal on Scientific Computing, 35 (2013), pp. B644–B665.
- [2] S. KINDERMANN, L. D. MUTIMBU, AND E. RESMERITA, *A numerical study of heuristic parameter choice rules for total variation regularization*, Journal of Inverse and Ill-Posed Problems, 22 (2013), pp. 63–94.
- [3] F. NATTERER, *The mathematics of computerized tomography*, vol. 32 of SIAM Classics in Applied Mathematics, SIAM, 2001.
- [4] K. NIINIMÄKI, M. LASSAS, K. HAMALAINEN, A. KALLONEN, V. KOLEHMAINEN, E. NIEMI AND S. SILTANEN, *Multi-resolution parameter choice method for total variation regularized tomography*, arXiv:1407.2386 [math.NA]
- [5] Y.-W. WEN AND R. CHAN, *Parameter selection for total-variation-based image restoration using discrepancy principle*, Image Processing, IEEE Transactions on, 21 (2012), pp. 1770–1781.

## Resolution-controlled conductivity discretization in electrical impedance tomography

ANDREAS RIEDER

(joint work with Robert Winkler)

In electrical impedance tomography (EIT) one wants to recover an isotropic conductivity distribution  $\sigma: \Omega \rightarrow [c_0, \infty[$ ,  $c_0 > 0$ , in the interior of an object  $\Omega \subset \mathbb{R}^2$ , e.g., a cross section of the human body. To this end, electric current is applied on the boundary of the object through electrodes and the resulting voltages are recorded at these electrodes as well.

The most accurate model for EIT to date is the *complete electrode model* (CEM) which we describe now in its variational formulation: Let  $\Omega$  be a simply connected Lipschitz domain and let  $E_j \subset \partial\Omega$ ,  $j = 1, \dots, L$ , denote the distinct electrodes having positive surface measure. With this electrode configuration we associate the electrode space

$$\mathcal{E}_L := \text{span}\{\chi_{E_1}, \dots, \chi_{E_L}\} \cap L^2_\diamond(\partial\Omega) \subset L^2_\diamond(\partial\Omega)$$

where  $\chi_{E_j}$  is the indicator function of  $E_j$  and  $L^2_\diamond(\partial\Omega)$  is the space of  $L^2$ -functions with vanishing mean along the boundary. The forward problem now reads: Given an electrode current  $I \in \mathcal{E}_L$  and a contact impedance  $z > 0$ , find a voltage potential  $u_p \in H^1(\Omega)$  and an electrode voltage  $U \in \mathcal{E}_L$  such that

$$a((u_p, U), (w, W)) = \int_{\partial\Omega} I W \, dS \quad \text{for all } (w, W) \in H^1(\Omega) \oplus \mathcal{E}_L$$

where the bilinear form  $a$  on  $H^1(\Omega) \oplus \mathcal{E}_L$  is defined by

$$a((v, V), (w, W)) := \int_{\Omega} \sigma \nabla v \nabla w \, dx + \frac{1}{z} \int_{\cup_j E_j} (v - V)(w - W) \, dS.$$

The above problem has a unique solution [5].

The nonlinear forward operator describing CEM is the *Neumann-to-Dirichlet map*  $R: \mathcal{D}(R) \subset L^\infty(\Omega) \rightarrow \mathcal{L}(\mathcal{E}_p)$ ,  $\sigma \mapsto \{I \mapsto U\}$ , where  $\mathcal{D}(R) = \{\sigma \in L^\infty(\Omega) : \sigma \geq c_0\}$ , that is,  $R(\sigma)I = U$ . Finally, we can phrase the inverse problem of EIT as the reconstruction of  $\sigma$  from the knowledge of  $R(\sigma)$ . Besides its illposedness this inverse problem suffers from too few measurements. Indeed, since  $R(\sigma)$  can be represented by a symmetric matrix of order  $L-1 = \dim \mathcal{E}_L$  we only have  $L(L-1)/2$  independent measurements.

To bring the best out of the measurements a sensible discretization of the conductivity is required. Conductivity discretizations have been considered before, see, e.g., [1, 2, 4] to name a few, but an explicit resolution-based quantification of the discretization size for CEM across  $\Omega$  is still an open task. In the remainder of this extended abstract we summarize our contribution to this task.

Motivated by Isaacson [3] we define the *relative sensitivity* for distinguishing the conductivity  $\tilde{\sigma}$  from the reference or background conductivity  $\sigma$  by

$$\lambda_{\sigma, \tilde{\sigma}} := \frac{\|R(\tilde{\sigma}) - R(\sigma)\|}{\|R(\sigma)\|}$$

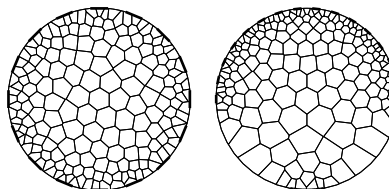
where  $\|\cdot\|$  denotes the spectral norm. We say that the conductivities  $\sigma$  and  $\tilde{\sigma}$  are *distinguishable* by the measurement device if  $\lambda_{\sigma, \tilde{\sigma}} \geq \varepsilon$  where  $\varepsilon \in ]0, 1[$  is the relative spectral measurement noise.

If  $\Omega$  is a circular disk we derived in [6] a procedure to calculate  $\lambda_{1, \tilde{\sigma}}$  explicitly for the circular inclusion  $\tilde{\sigma} = \tilde{\sigma}(x, r) = 1 + \eta \chi_{B_r(x)}$ ,  $\eta > 0$ , under any electrode configuration on  $\partial\Omega$  ( $B_r(x) \subset \Omega$  is the ball of radius  $r$  and center  $x$ ). For a large  $\eta$ , say  $\eta = 10^6$ , and a given relative measurement noise  $\varepsilon$  we are now able to determine the smallest radius  $r_{\min} = r_{\min}(x, \varepsilon)$  such that

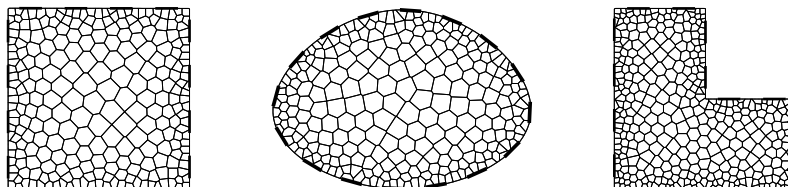
$$\varepsilon = \lambda_{1, \tilde{\sigma}(x, r_{\min})}.$$

The area of  $B_{r_{\min}}(x)$  is a characteristic of the resolution provided by CEM in  $x$  under the sensitivity/spectral noise level  $\varepsilon$ .

To obtain a mesh in  $\Omega$  where all cells have roughly the same impact on the measurements we pack  $\Omega$  with balls of the same sensitivity and use their centers as seeds of a Voronoi tessellation. We call the resulting meshes *optimal*. Two optimal meshes for  $\varepsilon = 0.02$  and for different electrode configurations are displayed on the right. The electrodes are indicated by bold segments.



By a heuristic we have been able to extend the concept of optimal meshes to general simply connected domains. Below you find such meshes for 16 electrodes and a relative sensitivity  $\varepsilon = 0.02$ .



Conductivity reconstructions on optimal meshes using synthetic and measured data are reported in [6].

#### REFERENCES

- [1] L. Borcea, V. Druskin, F. Guevara Vasquez, *Electrical impedance tomography with resistor networks*, Inverse Problems **24** (2008), 035013.
- [2] M. Cheney, D. Isaacson, J. Newell, S. Simske, J. Goble, *Noser: An algorithm for solving the inverse conductivity problem*, Inter. J. Imaging Sys. Techn. **2** (1990), 66–75.
- [3] D. Isaacson, *Distinguishability of conductivities by electric current computed tomography*, IEEE Trans. Med. Imaging **5** (1986), 91–95.
- [4] H. MacMillan, T. Manteuffel, S. McCormick, *First-order system least squares and electrical impedance tomography*, SIAM J. Numer. Anal. **42** (2004), 461–483.
- [5] E. Somersalo, M. Cheney, and D. Isaacson, *Existence and uniqueness for electrode models for electric current computed tomography*, SIAM J. Appl. Math. **52** (1992), 1023–1040.
- [6] R. Winkler, A. Rieder, *Resolution-controlled conductivity discretization in electrical impedance tomography* SIAM J. Imaging Sci. (2014, to appear).

## Time reversal and Cormack's last paper

VICTOR PALAMODOV

### 1. Time reversal (in the spirit of M. Fink) [1]

Let  $H \subset R^n$  be an open set (called cavity) in such that  $\partial H \subset Z$ , where  $Z$  be a hypersurface (called mirror).

An arbitrary function  $f$  supported by  $H$  is transmitted in a homogeneous medium to the manifold  $R_+ \times Z$ , the result is filtered by an operator  $F$  acting in  $R_+ \times Z$ , time reversed and retransmitted and detected as a function  $g$ . A reconstruction is given in the form  $Tf = pg$  for a known positive function  $p$  in  $H$  depending only on the geometry.

**2. Theorem.** The reconstruction is exact that is  $Tf = f$  if  $p$  is an arbitrary oscillatory polynomial and  $Z$  is the zero set of  $p$  with the density  $dZ = dx/dp$  and  $H$  is the hyperbolic cavity of  $p$ . The filtration operator  $F$  is a universal second order selfadjoint "vertical" operator acting in  $R_+ \times Z$  [2],[3].

**3. Oscillatory sets.** Let  $p$  be a real polynomial in  $R^n$  of degree  $m$  with the zero set  $Z$ . They are called *oscillatory* with respect to a cavity  $H \subset R^n \setminus Z$  if  $p$  has  $m$  simple zeros in  $L$  for almost any line  $L \subset R$  that meets  $H$ . *Hyperbolic cavity* of an oscillatory set  $Z$  any maximal connected cavity. There is only one bounded hyperbolic cavity, if  $Z$  is compact that is  $p$  is elliptic. Any hyperbolic cavity is convex.

**4. Examples.** Any ellipsoid, elliptic paraboloid, elliptic and parabolic cylinder is oscillatory with only one hyperbolic cavity. Two sheet hyperboloid is oscillatory with two hyperbolic cavities. If  $P = P(t, x)$  is a homogeneous polynomial in  $R^{n+1}$  that is hyperbolic with respect to  $t$  in the sense of I. Petrovsky, then the polynomial  $p(x) = P(1, x)$  is oscillatory in  $R^n$ . For arbitrary  $n, m \geq 2$  the set of oscillatory polynomials of  $n$  variables of degree  $m$  depends on several discrete and continual parameters.

**5. Reconstruction from spherical means.** This result is equivalent to some explicit FBP formulas for reconstruction of a function supported in  $H$  from data of spherical integrals for spheres with centers in  $Z$  [2],[3].

**6. The last paper of Allan Cormack.** Cormack proposed a method for determination of distribution of a scattered material by filtering the scattered light on travel times. "Suppose that waves travel in this space with a speed  $v$  and that the space contains a distribution of scattering material with a density  $f$  which is assumed to be smooth and either rapidly decreasing or of compact support... An impulsive plane wave front with a normal  $\omega$  reaches 0 at  $t = 0$ . As result of the well-known focusing property of paraboloids the scattering waves arriving at 0 at time  $t = 2p/v$  will all have originated on the paraboloid defined by  $r(1 + \langle \xi, \omega \rangle) = 2p$ ..." The mathematical problem is to reconstruct a function in a space from data of integrals over a family of confocal parabolas or confocal paraboloids. A reconstruction for this acquisition geometry is given by an explicit FBP formula [2],[4].

## REFERENCES

- [1] M. Fink and C. Prada, Acoustic time-reversal mirrors. *Inverse Probl.* 17 (2001), R1–R38.
- [2] V. P. Palamodov, A uniform reconstruction formula in integral geometry. *Inverse Probl.* 28 (2012) 065014.
- [3] V. P. Palamodov, Time reversal in photoacoustic tomography and levitation in a cavity. arxiv: 1405.6283
- [4] V. P. Palamodov, A. Cormack last inversion formula and a FBP reconstruction. arxiv: 1407.8473

**On artifacts in the limited data problem of spherical Radon Transform**

LINH NGUYEN

Let  $S$  be a smooth closed surface in  $\mathbb{R}^n$ . We consider the following restricted spherical Radon transform

$$R(f)(z, r) = \int_{\mathbb{S}(z, r)} f(y) d\sigma(y), \quad (z, r) \in S \times \mathbb{R}_+.$$

Here,  $\mathbb{S}(z, r)$  is the sphere of radius  $r$  centered at  $z$ . This transform appears in several imaging modalities, such as thermo/photo-acoustic tomography, ultrasound tomography, SONAR, and Inverse Elasticity.

The problem of inverting  $R$  has attracted intensive studies in the last decade. A comprehensive reference list can be found in [4]. In this talk, we discuss the microlocal analysis of a reconstruction formula with an emphasis on limited data problem.

Let us assume that  $S$  is the boundary of a convex domain  $\Omega$ . We consider the following operators:

$$P(h)(r) = \int_{\mathbb{R}} \int_0^{\infty} e^{i(\tau^2 - r^2)\lambda} |\lambda|^{n-1} h(\tau) d\tau d\lambda.$$

and

$$B(g)(x) = \frac{1}{2\pi^n} \int_S g(z, |z - x|) \langle z - x, \nu_z \rangle d\sigma(z).$$

Here,  $\nu_z$  is the outward normal of  $S$  at  $z$ . Then, if  $f$  is supported inside  $\Omega$ ,

$$BPR(f)(x) = f(x) + K(f)(x), \quad \text{for all } x \in \Omega,$$

where  $K$  is a pseudo-differential operator of order  $-1$  (see [3, 1, 2, 4]). Moreover,  $K \equiv 0$  if  $S$  is a sphere or an ellipse/ellipsoid (see [3, 1, 2]).

Let  $\Gamma$  be a proper subset of  $S$  with smooth boundary. Assume that we only know  $R(f)(z, r)$  for  $z \in \Gamma$ . That is, we only have **limited data**. Up to now, there is no closed form formula to find  $f$  from the limited data. In order to reconstruct the visible singularities of  $f$ , the following formula has been proposed

$$T(f)(x) := B_{\Gamma} PR(f)(x),$$

where

$$B_{\Gamma}(h)(x) = \frac{1}{2\pi^n} \int_{\Gamma} g(z, |z-x|) \langle z-x, \nu_z \rangle d\sigma(z).$$

Then,  $T(f)$  reconstructs all the visible singularities of  $f$  with the correct order. However, it also creates artifacts by rotating each (so-called) boundary singularity around the corresponding boundary point of  $\Gamma \subset S$ . These artifacts are  $\frac{1}{2}$ -order smoother than the (original) boundary singularity. Detailed results can be found in [5, 6].

Similar results for the case that  $\Gamma$  does not have smooth boundary can be found in [5].

#### REFERENCES

- [1] M. Haltmeier, *Inversion of circular means and the wave equation on convex planar domain*, *Computers & Mathematics with Applications* **65** (3) (2013), 1025–1036.
- [2] M. Haltmeier, *Universal Inversion Formulas for Recovering a Function from Spherical Means*, *SIAM Journal on Mathematical Analysis* **46** (1) (2014), 214–232.
- [3] F. Natterer, *Photo-acoustic inversion in convex domains*, *Inverse Problems and Imaging* **6** (2012), 315–320.
- [4] L.V. Nguyen, *On a reconstruction formula for spherical Radon transform: a microlocal analytic point of view*, *Analysis and Mathematical Physics* **4** (3) (2014), 199–220.
- [5] L.V. Nguyen, *On Artifacts in Limited Data Spherical Radon Transform I: Flat Observation Surfaces*. arXiv preprint at arXiv:1407.4496 .
- [6] L. Barannyk, J. Frikel, and L.V. Nguyen, *On Artifacts in Limited Data Spherical Radon Transform: Curved Observation Surfaces*. Preprint.

### PET imaging of freely moving mice via image registration

FRANK WÜBBELING

(joint work with Xiaoyi Jiang, Dirk Mannweiler, Julian Rasch, Klaus Schäfers, and Sönke Schmid)

Positron Emission Tomography (PET) is an excellent tool for viewing the metabolism of a live organism. Basically, a radioactive tracer is injected which accumulates for example at tumor cells. The emitted photons are detected, yielding the information that a decay took place on a line of response. In the limit of number of photons going to infinity, the Radon transform of the distribution function of the tracer is measured on a grid, and standard Radon inversion techniques could be used [7]. However, since radiation and acquisition time are limited, in practice these measurements are heavily corrupted by Poisson noise, which is taken into account by the selection of appropriate statistical reconstruction algorithms [10].

So acquisition time is a crucial parameter for image quality. It is easily around 15 minutes. Therefore, in small animal imaging e.g. mice are typically anaesthetized before studies are done. This prevents the application of PET as a quantitative method to analyze organ function that are affected by anesthesia (see eg. [1]), in particular brain activity. Thus, PET imaging of conscious, preferably even

freely moving, animals is highly desirable and currently being tried using dedicated instruments, see e.g. [5], [9], [4].

We present an alternative that does not employ specialized scanners, and which was tested with the QuadHIDAC wire chamber scanner. It is based on an algorithmical, mathematical approach, and demonstrates the value of the integration of image analysis tools into reconstruction algorithms. We give a purely technical description of what is done, the exact choices for mathematical modeling and implementation can be found in the cited literature. The procedure is

- (1) Take a normal PET scan of a freely moving mouse (it is in a cage).
- (2) Determine the motion of the mouse during the scan.
- (3) Perform a motion corrected, EM-based reconstruction.

For (1), an appropriate cage was built, equipped with four optical cameras which are used for mouse localization and motion detection, employing feature point algorithms. For the reconstruction part, the algorithms implemented in EMrecon [3] were used.

Optical Tracking provides only surface information. Since for PET reconstruction we also need the interior motion, it has to be estimated, resulting in unsatisfactory accuracy.

To deal with this, we propose to complement the video with additional information delivered by volume preserving registration algorithms, like they are used in human PET motion correction [2].

Observation of mice in the cage during the PET acquisition shows that in about 40 percent of the time, the mice are not moving at all. These static phases range from around 5 to 30 seconds. In order to derive information about interior motion, the following algorithm is applied.

- (1) Using the video tapes, extract scenes without motion, meaning extract scenes that change by less than a certain threshold in an appropriate norm.
- (2) From the low-SNR data acquired in these short scenes, reconstruct preliminary reconstructions. Note that due to the SNR, these will hardly be quantitative. EMTV-type algorithms are used for this [8].
- (3) Use image registration of the low quality images to derive motion of the interior of the mouse, VAMPIRE [2] and FAIR [6] were employed.
- (4) Use the motion information to reconstruct a quantitative image from all data acquired [3].

As a conclusion, the algorithm generally delivers quantitative results provided the mice are not running around too erratically. However, it turns out that the brain, which is the actual target, is extremely difficult to image, so that here the outcome is still unclear. Currently, the algorithm is in pre-clinical testing.

#### REFERENCES

- [1] M. Desai et al., *Mapping brain networks in awake mice using combined optical neural control and fMRI*, J Neurophysiol. 2011 Mar;105(3):1393-405.

- [2] Gigengack F, Ruthotto L, Burger M, Wolters CH, Jiang X, Schäfers K, *Motion correction in dual gated cardiac PET using mass-preserving image registration*, IEEE Transactions on Medical Imaging (2012), 31(3): 698–712
- [3] Kösters T, Schäfers K, Wübbeling F, *EMRecon: an expectation maximization based image reconstruction framework for emission tomography data (2011)*, Proceedings of IEEE Medical Imaging Conference, Valencia
- [4] Kyme A, Meikle S, Baldock C, Fulton R (2012), *Refraction-compensated motion tracking of unrestrained small animals in positron emission tomography*, Medical Image Analysis 16:1317–1328.
- [5] Mizuma H et al. (2010) *Establishment of in vivo brain imaging method in conscious mice* J Nucl Med 51:1068-1075.
- [6] J. Modersitzki, *FAIR: Flexible Algorithms for Image Registration* Philadelphia: SIAM, 2009.
- [7] Natterer F, Wübbeling F, *Mathematical Methods in Image Reconstruction*, SIAM 2001.
- [8] Sawatzky, Alex; Brune, Christoph; Wübbeling, Frank; Kösters, Thomas; Schäfers, K.; Burger, M. *Accurate EM-TV algorithm in PET with low SNR*, Nuclear Science Symposium Conference Record, 2008. NSS '08. IEEE , vol., no., pp.5133,5137, 19-25 Oct. 2008
- [9] Schulz D et al. *Simultaneous assessment of rodent behavior and neurochemistry using a miniature positron emission tomography*, Nature Methods 2011 8(4):347-352.
- [10] Shepp L., Vardi Y. *Maximum likelihood reconstruction for emission tomography*. Medical Imaging, IEEE Transactions on, 1982, 1(2):113:122.

## A Nonlinear Variational Approach to Motion-Corrected Reconstruction of Density Images

SEBASTIAN SUHR

(joint work with Martin Burger, Jan Modersitzki)

### MODELLING AND ANALYSIS

In our setup, we will be concerned with reconstruction a sequence of probability densities  $\rho_0, \dots, \rho_N$  on  $\Omega \subset \mathbb{R}^d$ , typically  $d = 2, 3$  such that

$$(1) \quad \rho_k(x) = \rho_0(y_k(x)) \det(\nabla y_k(x)),$$

with a reasonably smooth deformation field  $y_k$ . The measurements  $f_k$  are noisy versions of  $K(\rho_k)$ , with a stationary forward operator  $K$ , e.g. a convolution in fluorescence microscopy or versions of the x-ray transform in PET and SPECT.

We are going to minimize a problem of the form

$$(2) \quad J(\rho, y) = \sum_{k=0}^N (D(K\rho_k, f_k) + \alpha_k R_I(\rho_k) + \beta_k R_M(y_k)),$$

subject to (1). Here  $D$  is the data fidelity between estimated and measured data, and  $R_I$  respectively  $R_M$  are regularization functionals on the image respectively motion (with nonnegative regularization parameters  $\alpha_k$  and  $\beta_k$ ).

Since we aim at reconstructing images with sharp edges we employ total variation regularization ([1]) on the image, while we choose hyperelastic regularization ([2]) for the motion field. In detail the hyperelastic energy is given by

$$(3) \quad S^{\text{hyper}}(y) = \int_{\Omega} \alpha_1 \text{len}(\nabla y) + \alpha_2 \text{surf}(\text{cof}(\nabla y)) + \alpha_3 \text{vol}(\det(\nabla y)) dx ,$$

with the penalty functions

$$\text{len}(s) = \|s - \mathcal{I}\|_{\text{Fro}}^2, \quad \text{surf}(s) = (\|s\|_{\text{Fro}}^2 - 3)^2, \quad \text{vol}(s) = \frac{(s - 1)^4}{s^2} .$$

The three terms punish deviations from the identity and in volume, length and surface. Thus non local diffeomorphic transformations lead to infinite energies. Unfortunately there are some non global injective transformations, which are locally injective everywhere.

We turn our focus on the analysis of the presented model. If we follow the direct method in the calculus of variations, there are two properties of the functional to be proved:

- Coercivity
- Lower semi-continuity

While coercivity can be obtained from the chosen regularization functionals the proof of lower semi-continuity is challenging. For weakly convergent sequences

$$\rho_k \rightharpoonup^* \rho \text{ in BV} \quad y_k \rightharpoonup y \text{ in } H^1$$

we need to prove at least weak convergence, i.e:

$$(4) \quad \rho_k(y_k) \det(\nabla y_k) \rightharpoonup \rho(y) \det(\nabla y) \text{ in } L^1$$

For this we need a changes of variables, but unfortunately the transformation theorem for integrals does not hold in general. Therefore we use a generalized form, the area formula ([5])

$$(5) \quad \int_E \rho(y) \det(\nabla y) dx = \int_{\mathbb{R}^n} \rho(x) N_f(x, E) dx$$

$N_y$  is the Banach Indicatrix and defined by:

$$(6) \quad N_f(x, E) := \text{card}(\{f^{-1}(x) \cap E\})$$

The crucial question is whether we can control the Banach Indicatrix in  $L^\infty$ . By using results from degree theory for Sobolev mappings ([4]) we can deduce this from the boundary behaviour of the mapping: An orientation preserving  $H^1$  mapping is injective, iff it is injective on the boundary.

The question whether we can establish a bound of the following type

$$(7) \quad \|N_y\|_\infty \leq C(R_M(y), \Omega)$$

remains open.

## NUMERICAL ASPECTS

Similar to [7] we choose an alternating minimization approach, to minimize a discretized version of the functional. This leads to a two step algorithm:

- (1) Reconstruction Step: Minimize with respect to  $\rho$  for fix  $y$
- (2) Motion Step: Minimize with respect to  $y$  for fix  $\rho$

The first step leads to a minimization problem of the following type:

$$\min_{\substack{\rho_0 \\ \rho \geq 0}} \sum_i D(K\rho_0(y(t_i))|det(Dy_i)|, f_i) + \alpha J(\rho_0)$$

This can be solved via reconstruction algorithms incorporating motion information ([3], [1]).

The reconstruction step boils down to:

$$\min_y \sum_{i=1}^{n-1} D(K\rho_0(y_i)|det(Dy_i)|, f_i) + \frac{\beta}{2} \sum_{i=1}^{n-1} R_M(y_i)$$

(8)

As all summands are independent, we have to solve  $n - 1$  registration problems. Although the distance measure is defined on the detector domain, this can be done with standard registration algorithms like [6].

While the implementation of both steps is well understood, the challenge lies in the enforcing of injective transformations. A simple way would be to choose Dirichlet boundary conditions with  $y|_{\partial\Omega} = \text{Id}$ , but this might be too restrictive. Thus the question of a generalized registration framework for injective transformations arises.

## REFERENCES

- [1] Christoph Brune, Alex Sawatzky, and Martin Burger. Bregman-EM-TV methods with application to optical nanoscopy. In *Scale Space and Variational Methods in Computer Vision*. Springer Berlin / Heidelberg, 2009.
- [2] M. Burger, J. Modersitzki, and L. Ruthotto. A hyperelastic regularization energy for image registration. *SIAM Journal on Scientific Computing*, 35(1):B132–B148, 2013.
- [3] Thomas Kösters et al. Combined AW-OSEM reconstruction and mass-preserving motion correction of PET data. In *The 12th International Meeting on Fully Three-Dimensional Image Reconstruction in Radiology and Nuclear Medicine*, 2013.
- [4] M. Giaquinta, G. Modica, and J. Soucek. Remarks on the degree theory. *Journal of Functional Analysis*, 125(1):172 – 200, 1994.
- [5] Piotr Hajłasz. Change of variables formula under minimal assumptions. *Colloq. Math.*, 64(1):93–101, 1993.
- [6] Jan Modersitzki. *FAIR: Flexible Algorithms for Image Registration*. SIAM, 2009.
- [7] B. A. Mair, David R. Gilland, and Jing Sun. Estimation of images and nonrigid deformations in gated emission ct. *IEEE Transactions on Medical Imaging*, 25:1130–1144, 2006.

**On the V-line Radon transform and its applications in imaging**

GAIK AMBARTSOUMIAN

(joint work with Rim Gouia-Zarrad, Sunghwan Moon)

Single scattering optical tomography uses light, transmitted and scattered through an object, to determine the interior features of that object. If the object has moderate optical thickness it is reasonable to assume that the majority of photons scatter once. Using collimated emitters and receivers one can measure the intensity of light scattered along various broken rays corresponding to the paths of such photons. These measurements are then used to recover the spatially varying coefficients of light absorption and/or light scattering. The latter task is mathematically equivalent to the problem of inversion of a generalized Radon transform integrating along V-shaped broken rays (see [2, 3, 5] and the references there).

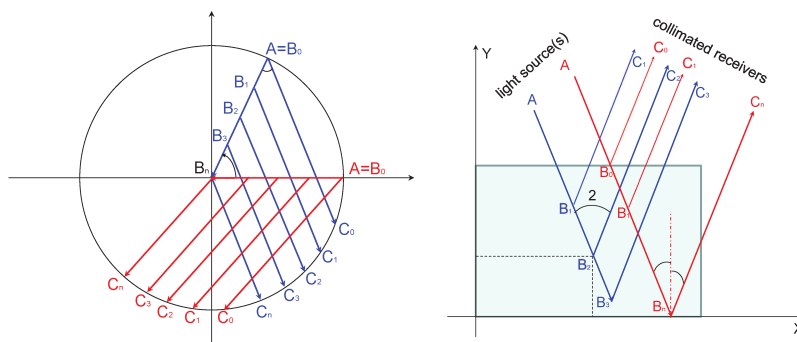
Since the family of broken rays in 2D is 4-dimensional, the inversion problem described above is overdetermined. Hence it is natural to consider the problem of inversion from integrals of image function along a 2D subset of broken rays.

**Definition 2.** *The V-line Radon transform (VRT) of function  $f(x, y)$  is the integral*

$$(1) \quad \mathcal{R}f(p_1, p_2) = \int_{BR(p_1, p_2)} f ds,$$

of  $f$  along the broken ray  $BR(p_1, p_2)$  with respect to line measure  $ds$ .

There are many ways to restrict the 4D family of broken-rays to a 2D subset. Motivated by geometric setups of other tomographic modalities, convenience of hardware implementation and symmetries simplifying the analysis, we consider below the cases of VRT in circular and rectangular geometries of data acquisition.



The left figure above describes the circular setup of VRT, where  $A(\phi)$  corresponds to the location of the light source, the points  $C_j = C(\phi, t_j)$  correspond to the locations of (an array of) receivers, and  $B_j = B(\phi, t_j)$  are the scattering points, where  $t_j$  is the distance from the breaking point to the origin. In the case of a fixed scattering angle  $\alpha \in (0, \pi/2)$  we have proved the following statement.

**Theorem 7.** [1] *If  $f(x, y)$  is a smooth function supported in the disc  $D(0, R)$ , then  $f$  is uniquely determined by  $\mathcal{R}f(\phi, t)$ ,  $\phi \in [0, 2\pi]$ ,  $t \in [0, R]$ .*

The proof of the theorem also provides an exact reconstruction formula of  $f$  from  $\mathcal{R}f(\phi, t)$  in this setup. Please see [1] for further details.

In the rectangular setup we consider broken rays with a fixed scattering angle  $2\beta$  symmetric with respect to  $y$ -axis (see the right-hand side figure above). Such rays can be uniquely parameterized by the Cartesian coordinates  $(x_v, y_v)$  of their vertices. In this case we have proved the following inversion result.

**Theorem 8.** [4] *Let  $f(x, y)$  be a smooth function supported in  $\mathcal{D} = \{(x, y) \in \mathbb{R}^2 \mid 0 \leq x \leq x_{max}, 0 \leq y \leq y_{max}\}$ . For  $(x_v, y_v) \in \mathbb{R}^2$  and fixed  $\beta \in (0, \frac{\pi}{2})$  denote  $g(x_v, y_v) = \mathcal{R}f(x_v, y_v)$ . Then*

$$f(x, y) = -\frac{\cos \beta}{2} \left[ \frac{\partial}{\partial y} g(x, y) + \tan^2(\beta) \int_y^{y_{max}} \frac{\partial^2}{\partial x^2} g(x, t) dt \right].$$

A natural generalization of the rectangular setup to 3D leads to consideration of the conical Radon transform (CRT). CRT integrates the image function of 3 variables over a 3D family of circular cones with fixed opening angle symmetric to the  $z$ -axis. Parameterizing each cone by the coordinates of its vertex  $(x_v, y_v, z_v)$  and denoting the CRT  $g(x_v, y_v, z_v) = \mathcal{R}f(x_v, y_v, z_v)$ , we prove the following statement.

**Theorem 9.** [4] *An exact solution of the inversion problem for CRT is given by*

$$\hat{f}_{\lambda, \mu}(z) = C(\beta) \int_{z_{max}}^z J_0(u(z-x)) \left[ \frac{d^2}{dx^2} + u^2 \right]^2 \int_{z_{max}}^x \hat{g}_{\lambda, \mu}(z_v) dz_v dx$$

where  $\hat{g}_{\lambda, \mu}(z_v)$  and  $\hat{f}_{\lambda, \mu}(z)$  are the 2D Fourier transforms of the functions  $g(x_v, y_v, z_v)$  and  $f(x, y, z)$  with respect to the first two variables,  $C(\beta) = \cos^2 \beta / (2\pi \sin \beta)$  and  $u = \tan \beta \sqrt{\lambda^2 + \mu^2}$ .

The author thanks the organizers of the Oberwolfach workshop ‘‘Mathematics and Algorithms in Tomography’’ for the invitation and opportunity to participate in such a great conference. He also expresses gratitude to the Mathematisches Forschungsinstitut Oberwolfach and US National Science Foundation for his travel support as a US Junior Oberwolfach Fellow. Part of this work was funded by NSF DMS-1109417 grant.

#### REFERENCES

- [1] G. Ambartsoumian and S. Moon, *A series formula for inversion of the V-line Radon transform in a disc*, Computers and Mathematics with Application, **66** (9), (2013), 1567–1572.
- [2] L. Florescu, V. A. Markel and J. C. Schotland, *Inversion formulas for the broken-ray Radon transform*, Inverse Problems **27** (2011), 025002.
- [3] L. Florescu, J. C. Schotland and V. A. Markel, *Single scattering optical tomography*, Phys. Rev. E **79** (2009), 036607.
- [4] R. Gouia-Zarrad and G. Ambartsoumian, *Exact inversion of the conical Radon transform with a fixed opening angle*, Inverse Problems **30** (2014), 045007.
- [5] A. Katsevich and R. Krylov, *Broken ray transform: inversion and a range condition*, Inverse Problems **29** (2013), 075008.

## Approximate marginalization of uninteresting unknowns in inverse problems

VILLE KOLEHMAINEN

(joint work with Jari P. Kaipio, Antti Nissinen)

In the Bayesian inverse problems framework, all unknown parameters are treated as random variables and all uncertainties can be modeled systematically. Recently, the approximation error approach has been proposed for handling modeling errors due to unknown nuisance parameters and model reduction [1, 2, 3]. In this approach, approximate marginalization of the modeling errors is carried out before the estimation of the interesting variables. In this talk, we describe the approximation error approach and present computational examples that are related to local X-ray tomography imaging and electrical impedance tomography.

### REFERENCES

- [1] Kaipio, J. and Somersalo, E. (2007). Statistical inverse problems: discretization, model reduction and inverse crimes. *J Comput Appl Math*, **198**.
- [2] Kolehmainen, V., Tarvainen, T., Arridge, S. R., and Kaipio, J. P. (2011). Marginalization of uninteresting distributed parameters in inverse problems – application to optical tomography. *Int. J. Uncertainty Quantification*, **1**(1), 1–17.
- [3] Jari Kaipio and Ville Kolehmainen. Approximate marginalization over modelling errors and uncertainties in inverse problems. In Paul Damien, Petros Dellaportas, Nicholas G. Polson and David A. Stephens, editors, *Bayesian Theory and Applications*. Oxford University Press (Oxford, UK), pages 644-672, (2013).

## Cone beam transverse ray transform

DAVID FINCH

(joint work with Patcharee Wongsason)

(Preliminary Report)

The object discussed in this talk is the transverse ray transform of a compactly supported vector field in Euclidean geometry. For a vector field  $f$ , point  $a$ , and direction  $\theta$ , the transverse ray transform of  $f$  at  $a$  in direction  $\theta$ , denoted  $\mathcal{T}f(a, \theta)$  is given by

$$(1) \quad \mathcal{T}f(a, \theta) = \int_0^\infty P_\theta f(a + t\theta) dt$$

where  $P_\theta$  denotes orthogonal projection on the subspace perpendicular to  $\theta$ . The transverse ray transform is complementary to the more frequently studied longitudinal or Doppler transform. The problem addressed is the recovery of a compactly supported vector field in three dimensional Euclidean space, from the data of its transverse ray transform for all points  $a$  lying in a space curve  $\Gamma$  and for all directions. Our arguments follow closely the work of Katsevich and Schuster, as presented at this workshop by Prof. Dr. Schuster. Under the assumption that  $f$  is  $C^2$  supported in the unit ball, and that  $\Gamma$  is a Tuy curve of order three with

respect to the ball, we show that  $f$  may be recovered by an explicit formula. The proof has three main steps. The first is to establish a Grangeat type formula, similar to that found by Kazantsev and Schuster for the Doppler transform, which relates the an operator applied to the tangential part of the Radon transform of  $f$  (taken componentwise) evaluated at  $(a \cdot \theta, \theta) \in R \times S^2$  to an operator applied to the transverse ray transform at  $a$ . Then, as for Katsevich and Schuster, combining the results for the several sources lying on the plane containing  $a$  with normal  $\theta$  allows to solve for the derivative of the tangential part of the Radon transform. This is the same intermediate data obtained by Katsevich and Schuster, so their method gives a formula to recover the solenoidal part of  $f$ . If  $f$  is written as  $f = \nabla\phi + f^s$  where  $\phi$  has compact support in the ball and  $f^s$  has zero divergence, then  $T\nabla\phi = \mathcal{D}\nabla\phi$ , where  $\mathcal{D}$  is the usual divergent beam x-ray transform. Any of the various reconstruction formulas for the cone beam transform may then be employed to recover  $\nabla\phi$ . Details will appear in a manuscript in preparation.

#### ACKNOWLEDGEMENT

DF was partially supported by NSF grant DMS-100914. PW was partially supported by a Royal Thai graduate fellowship.

#### REFERENCES

- [1] A. Katsevich and T. Schuster, *An exact inversion formula for cone beam vector tomography*, *Inverse Problems* **29** (2013), article id 065013.
- [2] P. Wongsason, *3D cone beam reconstruction formulas for the transverse-ray transform with source points on a curve*, PhD thesis, Oregon State University, (2014).

### **$\pi$ -line reconstruction formulas in tomography: numerical analysis of view dependent derivatives**

ADEL FARIDANI

(joint work with Ryan Hass)

Let

$$(1) \quad \mathcal{D}f(\mathbf{y}, \boldsymbol{\theta}) = \int_0^\infty f(\mathbf{y} + t\boldsymbol{\theta}) dt$$

denote the divergent beam transform. We are concerned with the numerical analysis of the view dependent derivative

$$(2) \quad \left. \frac{\partial}{\partial q} \mathcal{D}f(\mathbf{y}(q), \boldsymbol{\theta}) \right|_{q=s}$$

that occurs in so-called  $\pi$ -line inversion formulas for fan-beam and 3D helical tomography [1, 3, 4, 5, 8, 12].

For example, the derivative is present in the filtered-backprojection reconstruction formula

$$(3) \quad f(\mathbf{x}) = \frac{1}{2\pi^2} \int_{I_\pi(\mathbf{x})} \frac{1}{|\mathbf{x} - \mathbf{y}(s)|} \int_0^{2\pi} \frac{\partial}{\partial q} \mathcal{D}f(\mathbf{y}(q), \boldsymbol{\theta}(s, x, \gamma)) \Big|_{q=s} \frac{d\gamma}{\sin \gamma} ds$$

derived in [4], as well as in the backprojection-filtration formulas of [12]. It is worth noting that even in the 2D case where very good algorithms are available, algorithms based on (3) can offer advantages in some situations, for example when the x-ray source comes very close to the object. Furthermore, in our numerical experiments we found the convergence rate for smooth functions  $f$  to be the same as for the standard filtered backprojection algorithm. However, careful implementation of the derivative (2) has been found to be critical to achieve competitive performance of reconstruction algorithms. We present a detailed analysis for the well-known 2D fan-beam case with curved detector array and circular source curve. In this geometry one measures

$$g(s, \alpha) = \mathcal{D}f(\mathbf{y}(s), \boldsymbol{\theta}(s, \alpha))$$

where  $\mathbf{y}(s) = R(\cos s, \sin s)$ ,  $\boldsymbol{\theta}(s, \alpha) = \sin(\alpha)\mathbf{e}_u(s) + \cos(\alpha)\mathbf{e}_v(s)$ , with  $\mathbf{e}_u(s) = (-\sin s, \cos s)$ , and  $\mathbf{e}_v(s) = -\mathbf{y}(s)/|\mathbf{y}(s)| = -(\cos s, \sin s)$ . The view dependent derivative can now be expressed in terms of the detector coordinates  $(s, \alpha)$  and reads

$$(4) \quad \frac{d}{dq} \mathcal{D}f(\mathbf{y}(q), \boldsymbol{\theta}(s, \alpha)) \Big|_{q=s} = \frac{\partial g}{\partial s}(s, \alpha) + \frac{\partial g}{\partial \alpha}(s, \alpha).$$

We determine the leading error terms for several discretization schemes for (2) that have been proposed in the literature. Discretization schemes were generally classified in two distinct groups, depending on whether they were derived directly from (2) or from discretizing the right hand side of (4). For our analysis we use a unified framework by expressing all schemes in the second, chain rule based format. The detailed analysis can be found in our forthcoming paper [2]. Some of main results are as follows. In practice the sampling stepsize  $\Delta s$  is usually chosen much larger than  $\Delta \alpha$ . This choice is supported by the 2D sampling conditions for the divergent beam transform [7] and needs to be taken into account when discretizing (2). Indeed, our analysis shows that this is the main reason why the so-called direct scheme, a straightforward discretization of (2), does not give satisfactory results. The NPH scheme derived in [9] improved on the direct scheme but was later found to have non-isotropic resolution [11]. Our error analysis identifies the responsible error term. The ingenious NHDLH scheme [10] remedied this deficiency and set a new standard. Alternative and simpler improvements on the NPH scheme were the FHS [1] and the K [6] schemes. Our determination of the leading error terms for each scheme shows that the FHS scheme has the fewest error terms which are shared by most of the other schemes, each of which also has additional terms. Nevertheless, in our numerical experiments for this geometry the FHS, NHDLH, and K scheme give very comparable results. This is also true for numerical experiments for flat detectors and/or elliptical source curves as long

as the detector array is aligned perpendicular to the source position  $\mathbf{y}(s)$ . On the other hand, our experiments confirmed the findings in [10] that the NHDLH scheme gives clearly superior results in the particular case of an elliptical source curve and detector array aligned parallel to  $\frac{d}{ds}\mathbf{y}(s)$ . The reason for this is subject of our ongoing research.

#### REFERENCES

- [1] A. Faridani, R. Hass, and D.C. Solmon, D C, *Numerical and theoretical explorations in helical and fan-beam tomography*, Journal of Physics: Conference Series **124** (2008), 012024.
- [2] A. Faridani and R. Hass, *On numerical analysis of view dependent derivatives in computed tomography* (2014), submitted. Preprint available online at <http://people.oregonstate.edu/~faridana/preprints/preprints.html>
- [3] R. Hass and A. Faridani, *Regions of backprojection and comet tail artifacts for  $\pi$ -line reconstruction formulas in tomography*, SIAM J. Imaging Sci. **5** (2012), 1159–1184.
- [4] A. Katsevich, *Theoretically exact filtered backprojection-type inversion algorithm for spiral CT*, SIAM J. Appl. Math. **62** (2002), 2012–2026.
- [5] A. Katsevich, *An improved exact filtered backprojection algorithm for spiral computed tomography*, Advances in Applied Mathematics **32** (2004), 681–697.
- [6] A. Katsevich, *A note on computing the derivative at a constant direction*, Phys. Med. Biol. **56** (2011), N53–N61.
- [7] F. Natterer, *Sampling in fan-beam tomography*, SIAM J. Appl. Math. **53** (1993), 358–380.
- [8] F. Noo, M. Defrise, R. Clackdoyle, and H. Kudo, *Image reconstruction from fan-beam projections on less than a short scan*, Phys. Med. Biol., **47** (2002), 2525–2546.
- [9] F. Noo, J. Pack, and D. Heuscher, *Exact helical reconstruction using native cone-beam geometries*, Phys. Med. Biol. **48** (2003), 3787–3818.
- [10] F. Noo, S. Hoppe, F. Dennerlein, G. Lauritsch, and J. Hornegger, *A new scheme for view-dependent data differentiation in fan-beam and cone-beam computed tomography*, Phys. Med. Biol. **52** (2007), 5393–5414.
- [11] A. A. Zamyatin, K. Taguchi, and M. D. Silver, *Practical Hybrid Convolution Algorithm for Helical CT Reconstruction*, IEEE Trans. Nucl. Sci. **53** (2006), 167–174.
- [12] Y. Zou and X. C. Pan, *An extended data function and its generalized backprojection for image reconstruction in helical cone-beam CT*, Phys. Med. and Biol. **49** (2004), N383–N387.

### Quantum walks with discrete time

F. ALBERTO GRÜNBAUM

I will describe similarities and differences between classical random walks and quantum walks, their unitary counterparts. In particular they share a (properly interpreted) version of the renewal equation, and yet the importance of interference effects in the quantum case produces very strikingly different results. Some of these have intriguing topological interpretations. This is part of joint work with L. Velazquez, R. Werner, A. Werner, J. Bourgain and J. Wilkening. A couple of joint papers have appeared in the last two years in CMP.

*Reporter: Bernadette Hahn*

## Participants

**Prof. Dr. Gaik Ambartsoumian**

Department of Mathematics  
University of Texas at Arlington  
P. O. Box 19408  
Arlington, TX 76019-0408  
UNITED STATES

**Prof. Dr. Simon R. Arridge**

Department of Computer Science  
University College London  
Gower Street  
London WC1E 6BT  
UNITED KINGDOM

**Prof. Dr. K. Joost Batenburg**

Centrum Wiskunde & Informatica  
(CWI)  
Scientific Computing Group  
Science Park 123  
1090 GB Amsterdam  
NETHERLANDS

**Prof. Dr. Jan Boman**

Matematiska Institutionen  
Stockholms Universitet  
10691 Stockholm  
SWEDEN

**Prof. Dr. Martin Burger**

Institut für Numerische und  
Angewandte Mathematik  
Universität Münster  
Einsteinstr. 62  
48149 Münster  
GERMANY

**Prof. Dr. Rolf Clackdoyle**

Laboratoire Hubert Curien  
CNRS UMR 5516  
Campus Pole Opt. et Vision - Bat. F  
18, rue Prof. Benoit Laurus  
42000 St. Etienne  
FRANCE

**Prof. Dr. Michel Defrise**

Department of Nuclear Medicine  
Vrije Universiteit Brussel  
UZ Brussel  
Laarbeeklaan 101  
1090 Jette (Brussels)  
BELGIUM

**Prof. Dr. Laurent Desbat**

TIMC - IMAG  
Faculté de Médecine  
Université de Grenoble  
38706 La Tronche Cedex  
FRANCE

**Dr. Oliver Dorn**

School of Mathematics  
The University of Manchester  
Oxford Road  
Manchester M13 9PL  
UNITED KINGDOM

**Prof. Dr. Adel Faridani**

Department of Mathematics  
Oregon State University  
Kidder Hall 368  
Corvallis, OR 97331-4605  
UNITED STATES

**Prof. Dr. David V. Finch**

Department of Mathematics  
Oregon State University  
Kidder Hall 368  
Corvallis, OR 97331-4605  
UNITED STATES

**Dr. Jürgen Friel**

Institute of Computational Biology  
Helmholtz Zentrum München  
85764 Neuherberg  
GERMANY

**Prof. Dr. F. Alberto Grünbaum**

Department of Mathematics  
University of California  
Berkeley CA 94720-3840  
UNITED STATES

**Dr. Bernadette Hahn**

FR 6.1 - Mathematik  
Universität des Saarlandes  
Postfach 15 11 50  
66041 Saarbrücken  
GERMANY

**Prof. Dr. Per Christian Hansen**

DTU Compute  
Section for Scientific Computing  
Technical University of Denmark  
Bldg. 303  
2800 Lyngby  
DENMARK

**Prof. Dr. Ming Jiang**

Beijing International Center for  
Mathematical Research (BICMR)  
Peking University  
Beijing 100 871  
CHINA

**Prof. Dr. Alexander Katsevich**

Department of Mathematics  
University of Central Florida  
Orlando, FL 32816-1364  
UNITED STATES

**Dr. Holger Kohr**

Department of Mathematics  
KTH  
10044 Stockholm  
SWEDEN

**Prof. Dr. Ville Kolehmainen**

Inverse Problems Group  
Department of Applied Physics  
University of Eastern Finland  
Yliopistonranta 1E  
P.O. Box 1627  
70211 Kuopio  
FINLAND

**Prof. Dr. Leonid Kunyansky**

Department of Mathematics  
University of Arizona  
617 N. Santa Rita  
Tucson AZ 85721-0089  
UNITED STATES

**Dr. Aref Lakhali**

Institut für Angewandte Mathematik  
Universität des Saarlandes  
Postfach 151150  
66041 Saarbrücken  
GERMANY

**Prof. Dr. Armin Lechleiter**

Zentrum für Technomathematik  
FB 3, Universität Bremen  
Postfach 330 440  
28334 Bremen  
GERMANY

**Prof. Dr. Alfred K. Louis**

FR 6.1 - Mathematik  
Universität des Saarlandes  
66041 Saarbrücken  
GERMANY

**Dr. Linh Nguyen**

Department of Mathematics  
University of Idaho  
875 Perimeter Drive MS  
Moscow ID 83844  
UNITED STATES

**Dr. Clifford Nolan**

Department of Mathematics & Statistics  
University of Limerick  
Limerick  
IRELAND

**Dr. Steven Oeckl**

Fraunhofer EZRT  
Flugplatzstr. 75  
90768 Fürth  
GERMANY

**Dr. Ozan Öktem**

Department of Mathematics  
KTH  
10044 Stockholm  
SWEDEN

**Prof. Dr. Victor P. Palamodov**

School of Mathematical Sciences  
Tel Aviv University  
Ramat Aviv  
Tel Aviv 69978  
ISRAEL

**Dr. Sarah Patch**

Department of Physics  
University of Wisconsin-Milwaukee  
PO Box 413  
Milwaukee, WI 53201  
UNITED STATES

**Prof. Dr. Eric Todd Quinto**

Department of Mathematics  
Tufts University  
503 Boston Ave.  
Medford, MA 02155  
UNITED STATES

**Prof. Dr. Ronny Ramlau**

Industrial Mathematics Institute  
Johannes Kepler University  
Altenbergerstr. 69  
4040 Linz  
AUSTRIA

**Prof. Dr. Andreas Rieder**

Karlsruher Institut f. Technologie (KIT)  
Inst. f. Angew. & Numerische  
Mathematik  
76131 Karlsruhe  
GERMANY

**Dr. Gael Rigaud**

Fachrichtung Mathematik  
Universität des Saarlandes  
Postfach 151150  
66041 Saarbrücken  
GERMANY

**Alex Sawatzky**

Institute for Computational and Applied  
Mathematics - Imaging Workgroup  
Universität Münster  
Einsteinstr. 62  
48149 Münster  
GERMANY

**Prof. Dr. Otmar Scherzer**

Computational Science Center  
Universität Wien  
Nordbergstrasse 15  
1090 Wien  
AUSTRIA

**Prof. Dr. Carola-Bibiane  
Schoenlieb**

Department of Applied Mathematics and  
Theoretical Physics (DAMTP)  
Centre for Mathematical Sciences  
Wilberforce Road  
Cambridge CB3 0WA  
UNITED KINGDOM

**Tobias Schön**

Fraunhofer EZRT  
Flugplatzstr. 75  
90768 Fürth  
GERMANY

**Prof. Dr. John C. Schotland**

Department of Mathematics  
University of Michigan  
East Hall  
Ann Arbor, MI 48109-1109  
UNITED STATES

**Prof. Dr. Thomas Schuster**

Fachrichtung 6.1 - Mathematik  
Universität des Saarlandes  
Postfach 151150  
66041 Saarbrücken  
GERMANY

**Prof. Dr. Vladimir A.**

**Sharafutdinov**  
Novosibirsk State University  
Department of Mathematics &  
Mechanics  
Pirogova 2  
Novosibirsk 630 090  
RUSSIAN FEDERATION

**Prof. Dr. Samuli Siltanen**

Department of Mathematics & Statistics  
University of Helsinki  
P.O. Box 68  
00014 University of Helsinki  
FINLAND

**Sebastian Suhr**

Fachbereich Mathematik  
Universität Münster  
48149 Münster  
GERMANY

**Prof. Dr. Gunther A. Uhlmann**

Department of Mathematics  
University of Washington  
Padelford Hall  
Box 354350  
Seattle, WA 98195-4350  
UNITED STATES

**Dr. Frank Wübbeling**

Institut für Numerische und  
Angewandte Mathematik  
Universität Münster  
Einsteinstr. 62  
48149 Münster  
GERMANY